



CERN-EP-2021-144
18 July 2021

Measurement of very forward energy and particle production at midrapidity in pp and p–Pb collisions at the LHC

ALICE Collaboration*

Abstract

The very forward energy is a powerful tool for characterising the proton fragmentation in pp and p–Pb collisions and, studied in correlation with particle production at midrapidity, provides direct insights into the initial stages and the subsequent evolution of the collision. Furthermore, the correlation between the forward energy and the production of particles with large transverse momenta at midrapidity provides information complementary to the measurements of the underlying event, which are usually interpreted in the framework of models implementing centrality-dependent multiple parton interaction.

Results about the very forward energy, measured by the ALICE zero degree calorimeters (ZDC), and its dependence on the activity measured at midrapidity in pp collisions at $\sqrt{s} = 13$ TeV and in p–Pb collisions at $\sqrt{s_{NN}} = 8.16$ TeV are presented and discussed. The measurements performed in pp collisions are compared with the expectations of three hadronic interaction event generators: PYTHIA 6 (Perugia 2011 tune), PYTHIA 8 (Monash tune), and EPOS LHC. These results provide new constraints on the validity of models in describing the beam remnants at very forward rapidities, where perturbative QCD cannot be used.

1 Introduction

During the last decade, the study of bulk properties of proton–proton (pp) and proton–nucleus (pA) collisions at LHC energies has attracted increasing interest. Effects expected to occur only in heavy-ion collisions, such as collective fluid-like behaviour [1, 2] and strangeness enhancement [3], are already seen in pp collisions. In particular, the strangeness enhancement occurs already at small multiplicity values. The strength of these effects increases steadily with the final state multiplicity going from pp to p–Pb up to peripheral Pb–Pb collisions. As a consequence, minimum-bias (MB) pp collisions are currently being studied, focusing on the dependence of experimental observables on the charged-particle multiplicity measured at midrapidity. In phenomenological models inspired by quantum chromodynamics (QCD), high-multiplicity pp and pA events are generated in collisions with a smaller than average impact parameter, b (the distance between the centres of the two colliding hadrons). In these central collisions, the number of partonic interactions and, hence, the probability for partonic scatterings with large momentum transfer, is enhanced. On the other hand, by requesting the production of a particle with large transverse momentum, events with a larger than average multiplicity are selected [4]. In order to constrain the initial state of pp and p–Pb collisions, the correlation between observables measured in rapidity regions that are causally disconnected in the evolution of the system following the collision are studied. In particular, this is the case for the very forward (“zero degree”) energy and central rapidity particle production. The study of these correlations also addresses the fundamental question of how the energy of the colliding protons is transferred from beam to central rapidities. In models where the initial state is described by the impact parameter or initial matter overlap, an increased energy transfer results naturally from the increased number of parton–parton scatterings.

The processes involved in forward hadron production at high energies are also relevant for simulations of high-energy cosmic-ray interactions [5]. In particular, the production of forward baryons has a key role in the simulation of the development of cosmic-ray showers. Measurements at colliders can provide unique information for the tuning of hadronic interaction models that are widely used in this field.

In ALICE, the zero-degree calorimeters (ZDC) measure the energy carried by neutrons and protons emitted at rapidities close to that of the beam, covering projectile and target fragmentation regions. The very forward energy measured by the ZDC can be correlated with the charged-particle multiplicity and the probability of producing a particle with a large transverse momentum, p_T , at midrapidity. Measurements of very forward energy as a function of the p_T of the leading particle (the charged particle with the higher transverse momentum) at midrapidity complement the studies of the underlying event (UE). In the first case, particle production is related to an observable separated in pseudorapidity, while in the UE measurement particle production is measured in a region separated in azimuthal angle (“transverse region”). Another interesting effect discussed in the literature [6], that can be addressed with ZDC measurements, is the relation between the proton fragmentation in central pp collisions and the decrease in the energy carried forward by the leading baryons (baryons carrying a large fraction of the proton beam energy). This effect is predicted to occur along with an increased activity at midrapidity.

This article presents the first measurements of the dependence of the very forward energy on midrapidity particle production in pp collisions at a centre-of-mass energy $\sqrt{s} = 13$ TeV and in p–Pb collisions at a centre-of-mass-energy per nucleon pair $\sqrt{s_{NN}} = 8.16$ TeV. The article is organised as follows: in Sec. 2 the main ALICE subsystems used for this analysis are concisely described. The data sample, the event and track selection criteria are discussed in Sec. 3. Section 4 presents results about the production of energy at forward and backward rapidities in pp collisions. In Sec. 5 results on the correlation between very forward energy and particle production at midrapidity in pp and in p–Pb collisions are presented and discussed, together with results on the forward leading-baryon production in connection with the UE measurements in pp collisions.

Table 1: ZN and ZP event selection fractions (see text for details) in pp and p–Pb collisions. For the p–Pb colliding system, both the Pb-fragmentation (Pb) and the p-fragmentation (p) sides are reported.

	pp $\sqrt{s} = 13$ TeV	p–Pb $\sqrt{s_{NN}} = 8.16$ TeV
ZN	61%	96% (Pb) 43% (p)
ZP	23%	82% (Pb) 15% (p)

2 ALICE detectors

A detailed description of the ALICE detector and its performance can be found in Refs. [7, 8]. The sub-detectors used for the present analysis are the inner tracking system (ITS), the time projection chamber (TPC), the V0 detectors, all located inside a 0.5 T uniform magnetic field, and the ZDC.

The silicon pixel detector (SPD) [7] constitutes the two cylindrical innermost layers of the ITS and consists of hybrid silicon pixel assemblies covering the pseudorapidity range $|\eta| < 2$ for the inner layer and $|\eta| < 1.4$ for the outer layer for collisions occurring at the nominal interaction point (IP). The SPD is used to measure the charged-particle multiplicity at midrapidity using tracklets, short track segments formed using information on the position of the primary vertex and a couple of hits, registered on each of the SPD layers. To exploit the full particle tracking, the four external layers of the ITS, composed by two layers of silicon drift detectors (SDD) and two layers of double-sided silicon micro-strip detectors (SSD), were also used. The TPC [9] is the main tracking detector and it covers a pseudorapidity range of about $|\eta| < 0.9$. In order to avoid border effects, in this analysis the fiducial pseudorapidity region has been restricted to $|\eta| < 0.8$. Charged-particle tracks are formed by combining the hits in the ITS and the reconstructed clusters in the TPC. The trigger signal is provided by the V0 [10] counters, two arrays of 32 scintillator tiles each, covering the full azimuth within $-3.7 < \eta < -1.7$ for V0C, located on the same side as for the ALICE dimuon arm (C-side), and $2.8 < \eta < 5.1$ for V0A, placed on the opposite side (A-side). An alternative trigger condition can be provided by the ALICE diffractive (AD) detector [11], a hodoscope of plastic scintillators covering the pseudorapidity ranges $-4.9 < \eta < -7.0$ and $4.8 < \eta < 6.3$.

The main detectors used in this analysis are the ZDC. Two identical systems, each comprising a neutron (ZN) and a proton (ZP) calorimeter of the “spaghetti” type, are placed at ± 112.5 m from the ALICE IP, on both sides. Neutrons are detected in tungsten-quartz calorimeters, while protons in brass-quartz calorimeters. The ZN calorimeters cover the pseudorapidity range $|\eta| > 8.8$, while for the ZP calorimeters the geometric coverage is $6.5 < |\eta| < 7.4$, but the actual pseudorapidity coverage strongly depends on the LHC beam optics settings, since charged particles are deflected by the beam line magnetic fields. In nucleus–nucleus collisions, the ZDC detect the energy carried by the non-interacting (spectator) nucleons and they are used to estimate the centrality of the collision [12]. In proton–nucleus collisions the ZDC provide an unbiased centrality selection [13]. In proton–proton collisions, the ZDC are usually switched off, not only to prevent their aging but also because the typical beam conditions in pp data taking are characterised by large crossing angles that drastically affect the ZDC acceptance. In particular, the acceptance of ZN is not affected provided that the vertical half-crossing angle is smaller than $+60 \mu\text{rad}$ for a nominal vertex vertical position on the LHC axis ($y_{\text{vtx}} = 0$ mm).

The ZDC are equipped with time-to-digital converters (TDC) that register the arrival time of particles depositing energy in the detectors, allowing in addition the rejection of events without signal in the calorimeters. The event selection fractions for both ZN and ZP are defined as the ratios between the number of events with a signal in the corresponding TDC and the number of MB events triggered by ALICE. The event selection fractions values calculated for the two colliding systems are given in Table 1. In Pb–Pb collisions and in p–Pb collisions in the Pb-fragmentation region, the energy calibrations of ZN and ZP spectra are performed using the narrow peaks from the detection of single nucleons. Contrarily, in pp collisions and in p–Pb collisions in the p-fragmentation region, there are no peaks in the spectra and

there is no reliable way to calibrate the spectra in energy units without introducing model dependencies and large uncertainties. The use of self-normalised quantities, namely signals normalised to their average minimum-bias value, allows one to overcome this issue, since they coincide with the self-normalised energy ratios.

3 Data samples, event selection and models

During the 2015 pp data taking at $\sqrt{s} = 13$ TeV, the ZDC were switched on when a limited half-crossing angle of $+45 \mu\text{rad}$ in the vertical plane was applied. As discussed in the previous section, this configuration guaranteed that all the neutrons emitted at very forward rapidities were within the ZN geometric acceptance. Data from p–Pb collisions, collected in 2016 at centre-of-mass energy $\sqrt{s_{\text{NN}}} = 8.16$ TeV, were used to study the forward energy on the p-fragmentation side in pA collisions. The proton beam energy was the same as in pp collisions, therefore comparing the very forward energy in the p-fragmentation side in p–Pb collision to the one detected in pp collisions provides useful information on the proton breakup.

In both collision systems, a MB trigger condition, requiring at least one hit in both V0 detectors, was applied. The V0 timing information was used offline to reject beam–gas interactions. Events with more than one reconstructed primary interaction vertex (pile-up) were rejected. The selected events were required to have a reconstructed collision vertex with a position along the beam axis $|z_{\text{vtx}}| < 10$ cm to ensure a uniform performance for midrapidity detectors. After applying these selections, about 4×10^7 MB events in pp collisions and 8.3×10^7 MB events in p–Pb collisions were retained.

In the analysis of pp collisions, to study the transverse momentum of the leading particle, tracks were reconstructed in $|\eta| < 0.8$ applying more stringent quality selection criteria. To guarantee that all tracks have the maximal length, only those in the pseudorapidity interval $|\eta| < 0.8$ were selected. In order to ensure good track momentum resolution, the reconstructed tracks were required to have at least 70 reconstructed points (out of a maximum of 159) in the TPC, and two hits in the ITS, with at least one in the SPD. Finally, the χ^2 per TPC reconstructed point was required to be less than 4, and tracks originating from kink topologies of weak decays were rejected. The applied conditions selected tracks with a transverse momentum $p_{\text{T}} > 0.15$ GeV/c.

The very forward energy was studied as a function of the charged-particle multiplicity measured at midrapidity in $|\eta| < 1$. In p–Pb collisions, the nucleon–nucleon centre-of-mass system moves with respect to the ALICE laboratory system with a rapidity of -0.465 in the direction of the proton beam, and a pseudorapidity interval in the laboratory reference frame $|\eta_{\text{lab}}| < 1$ is used. The multiplicity selection is based on the number of tracklets measured in the SPD both in pp and in p–Pb collisions, as described in Refs. [14, 15]. The average charged-particle multiplicity values, $\langle dN_{\text{ch}}/d\eta \rangle$, are listed in Table 2 for each selected multiplicity interval. In addition, for p–Pb collisions a centrality selection based on ZN energy, that is the most unbiased selection available [13], was used to compare data at the two available centre-of-mass energies, $\sqrt{s_{\text{NN}}} = 5.02$ and 8.16 TeV.

Data from pp collisions are compared to Monte Carlo (MC) simulations using PYTHIA 6 (Perugia 2011 tune) [16], PYTHIA 8 (Monash 2013 tune) [17] and EPOS LHC [18] as event generators. The GEANT 3 [19] particle transport code was used to track particles through the ALICE experimental setup. PYTHIA 6.4 Perugia 2011 has a particular tune of the initial, final state showers and UE modelling. In particular, the tuning of the beam remnant is done using MB observables such as charged-particle multiplicity and transverse momentum spectra measured by CDF. In this tune, some early LHC data were used for the tuning of beam remnants. PYTHIA 8 Monash is the default tune of PYTHIA 8.1 which uses UE data from the LHC, SPS and Tevatron to tune the parameters relevant for multi-partonic interactions (MPI). No particular tune of the beam remnant is implemented. EPOS LHC is an update of the EPOS 1.99 model that uses early LHC data for tuning. For the midrapidity part, strings composed of pomerons can be exchanged in parallel for every event creating MPI. Instead, the beam remnants can

Table 2: Charged-particle multiplicity classes based on the SPD estimator and corresponding $\langle dN_{\text{ch}}/d\eta \rangle$ values in $|\eta| < 1$ in pp collisions at 13 TeV [14] (left table) and $|\eta_{\text{lab}}| < 1$ in p–Pb collisions at 8.16 TeV [15] (right table). The MB values for the two colliding systems are given in the bottom row.

Multiplicity class	pp 13 TeV $\langle dN_{\text{ch}}/d\eta \rangle$	Multiplicity class	p–Pb 8.16 TeV $\langle dN_{\text{ch}}/d\eta \rangle$
0–1%	$33.29^{+0.57}_{-0.51}$	0–1%	75.49 ± 2.01
1–5%	$23.44^{+0.37}_{-0.33}$	1–5%	57.26 ± 1.49
5–10%	$18.25^{+0.28}_{-0.25}$	5–10%	46.82 ± 1.22
10–15%	$15.13^{+0.22}_{-0.20}$	10–15%	40.57 ± 1.05
15–20%	$12.88^{+0.19}_{-0.17}$	15–20%	35.98 ± 0.94
20–30%	$10.50^{+0.16}_{-0.14}$	20–30%	30.70 ± 0.80
30–40%	$8.18^{+0.12}_{-0.11}$	30–40%	25.03 ± 0.66
40–50%	$6.30^{+0.10}_{-0.09}$	40–50%	20.22 ± 0.53
50–70%	4.13 ± 0.06	50–60%	15.92 ± 0.31
70–100%	1.87 ± 0.04	60–70%	11.71 ± 0.41
MB values	7.47 ± 0.11	70–100%	4.77 ± 0.15
		MB values	20.61 ± 0.62

derive from the decay of a resonance or from a string elongated along the beam axis if its mass is high enough.

4 Forward–backward energy asymmetry in pp collisions

The emission of very forward energy can be investigated over a pseudorapidity gap of more than 18 units using both ZDC systems, placed on the two sides relative to the IP. The correlation between the energy emitted at forward and backward rapidities in MB collisions is shown in Fig. 1, separately for ZN and ZP. In both cases, the detected energies show asymmetric features, namely a high energy deposit on one side corresponds to a very low energy deposition on the opposite side. In addition, a subset of the event sample is correlated, in particular for neutron emission. The origin of the observed asymmetry in energy at forward and backward rapidities was further investigated in MC generators, without considering any tracking through the experimental set-up, but selecting solely on particle kinematics. It was found that the energy emitted at large rapidities becomes asymmetric once the phase space is restricted for neutral particles to the pseudorapidity range covered by ZN and for charged particles to the nominal ZP pseudorapidity range. In conclusion, the observed asymmetry is an effect due to the limited and not overlapping pseudorapidity ranges covered by the neutron and the proton detectors.

To further characterise the forward–backward energy correlation, the asymmetry was calculated for ZN and ZP. The asymmetry can be calculated only for events with a signal either on the A or on the C-side, and is defined as:

$$\text{ZN asymmetry} = \frac{ZNA - ZNC}{ZNA + ZNC}, \quad \text{ZP asymmetry} = \frac{ZPA - ZPC}{ZPA + ZPC}$$

The asymmetry was calculated also for uncorrelated events, using a mixed-event technique, namely combining different (uncorrelated by definition) events for A and C side. Symmetric events are also present in the distribution as calculated from mixed events, as can be seen in Fig. 2. These symmetric events in the uncorrelated sample are an artifact due to the shape of ZN and ZP spectra, in which the

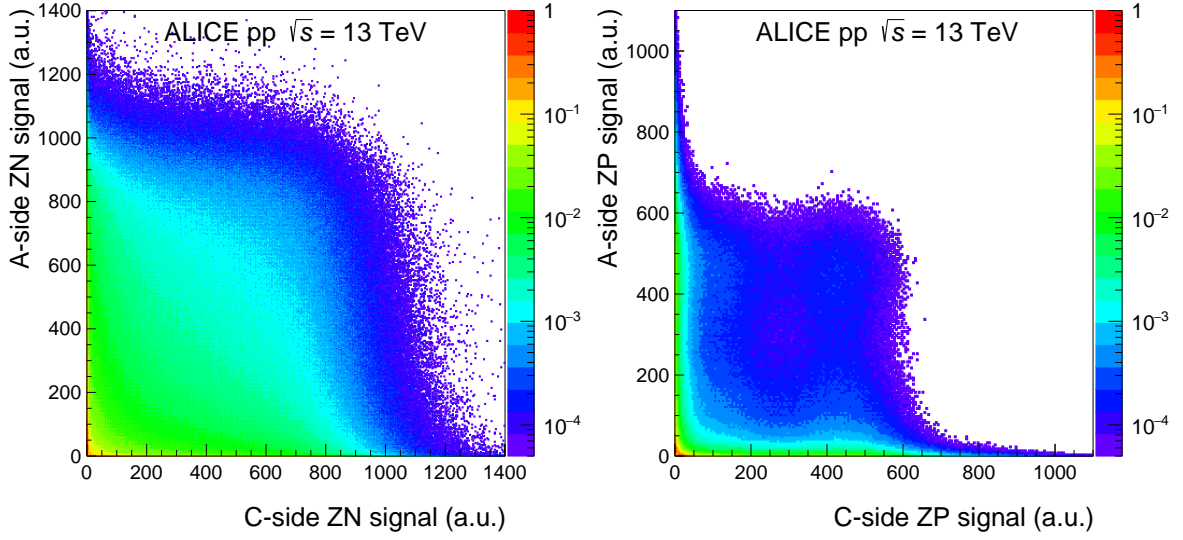


Figure 1: A- vs. C-side signal in ZN (left) and ZP (right). The maximum at (0,0) is normalised to unity, while the minimum is limited to 10^{-4} .

main contribution is provided by steeply falling spectra dominated by low energy values. This results in a high probability that two small energy values are randomly selected from uncorrelated events, resulting in a null asymmetry value. After subtracting the mixed event contribution from the same distribution, the prevailing feature remains the presence of asymmetric events, while the peak around null asymmetry is washed out both in data and in simulated events, as shown in the bottom panels of Fig. 2. Data for ZP are not fully symmetric relative to null asymmetry, showing a slightly larger amount of energy on the A side. The effect is below 1% and is imputed to a residual difference in A and C-side ZP spectra after the equalisation.

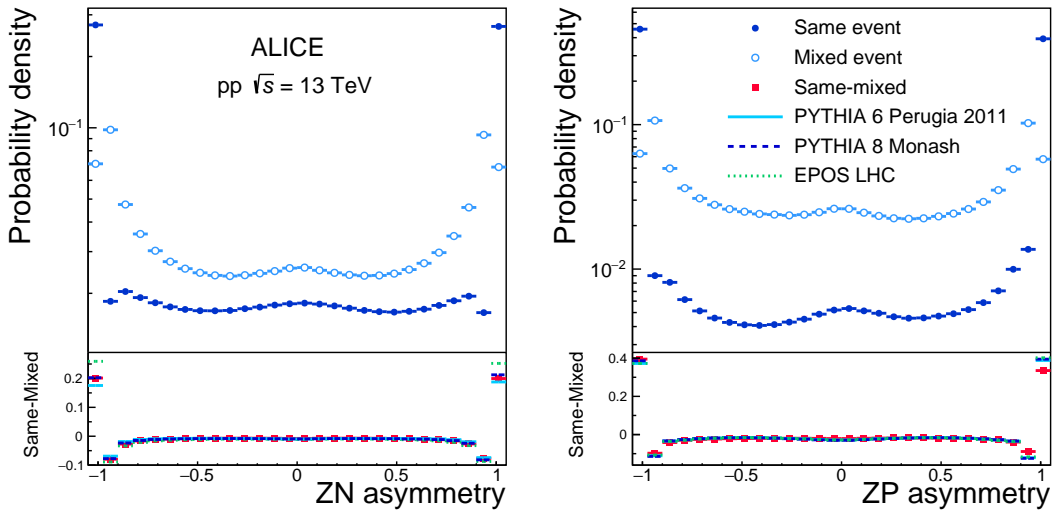


Figure 2: ZN (left) and ZP (right) asymmetry distributions for same (blue full circles) and mixed event distributions (blue open circles). In the bottom panels the difference between the uncorrelated and the correlated distributions is shown (red full squares) and compared to the simulation results using the three event generators (lines).

Another way to gain insight into the correlation between energy emitted at backward and forward rapidities is to study the average signal on one side as a function of the signal on the other side. Results are shown in Fig. 3, together with comparisons to model calculations. The energies carried by leading protons in the two sides are not correlated, as was already observed at lower energies at the ISR [20]. On the contrary, data indicate the presence of a correlation between the energies carried by leading neutrons on opposite sides, in particular at high energies. Models predict a flat behaviour for leading protons in good agreement with data, while for neutrons, even though they show some degree of correlation between the neutron energies, none of them is able to reproduce quantitatively the measured dependence over the whole range.

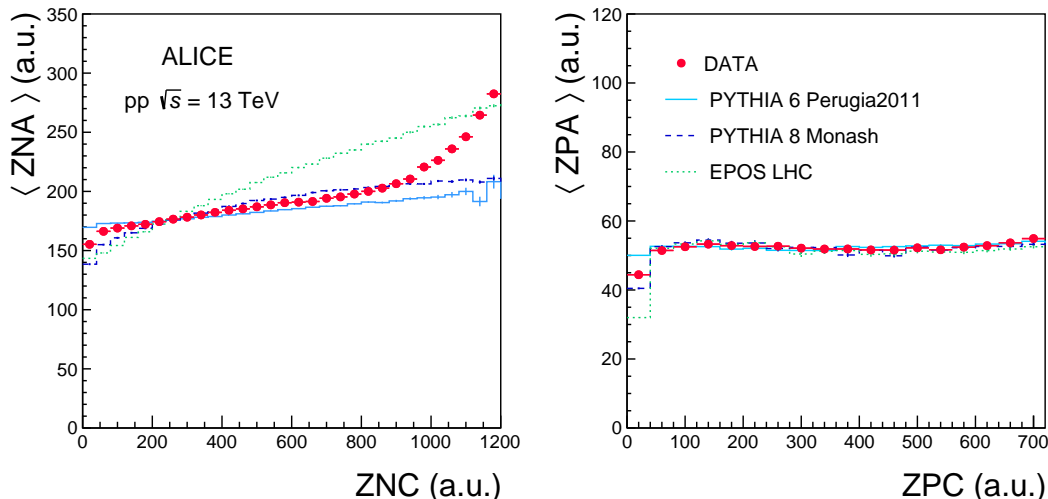


Figure 3: Average A-side ZN (left) and ZP (right) signals as a function of the C-side signals in pp collisions at $\sqrt{s} = 13$ TeV. Data (red full circles) are compared with model predictions from PYTHIA 6 (solid blue line), PYTHIA 8 (dashed blue line) and EPOS (dotted green line).

5 Forward energy as a function of charged-particle production at midrapidity

From phenomenological models one expects that selecting events characterised by a larger than average multiplicity or by the emission of a large transverse momentum particle corresponds to selecting collisions with a smaller than average impact parameter [21, 22], and a larger than average number of MPI [23]. The forward energy detected by the ZDC was studied as a function of the charged-particle multiplicity produced at midrapidity (in $|\eta| < 1$ for pp collisions at $\sqrt{s} = 13$ TeV and $|\eta_{\text{lab}}| < 1$ for p–Pb collisions at $\sqrt{s_{\text{NN}}} = 8.16$ TeV), and as a function of the leading particle transverse momentum, $p_{\text{T}}^{\text{leading}}$, in $|\eta| < 0.8$ in pp collisions. To study the interaction of a proton either with another proton or with a Pb nucleus, the dependence of the very forward energy on charged particle production at midrapidity was studied in both pp and p–Pb collisions.

5.1 Very forward energy in p–Pb collisions

In p–Pb collisions, the p-fragmentation and the Pb-fragmentation sides show a complementary behaviour as a function of centrality, as already reported for $\sqrt{s_{\text{NN}}} = 5.02$ TeV p–Pb collisions [13]. In Fig. 4, the self-normalised ZN signals as a function of centrality, estimated through the energy measured in the Pb-fragmentation region as described in Ref. [13], are shown for the Pb-fragmentation and for the p-fragmentation sides. Events characterised by a large multiplicity (corresponding to central events)

have a large forward energy deposit in the Pb-fragmentation side and a small energy deposit in the p-fragmentation side. This behaviour does not show a strong dependence on the collision energy.

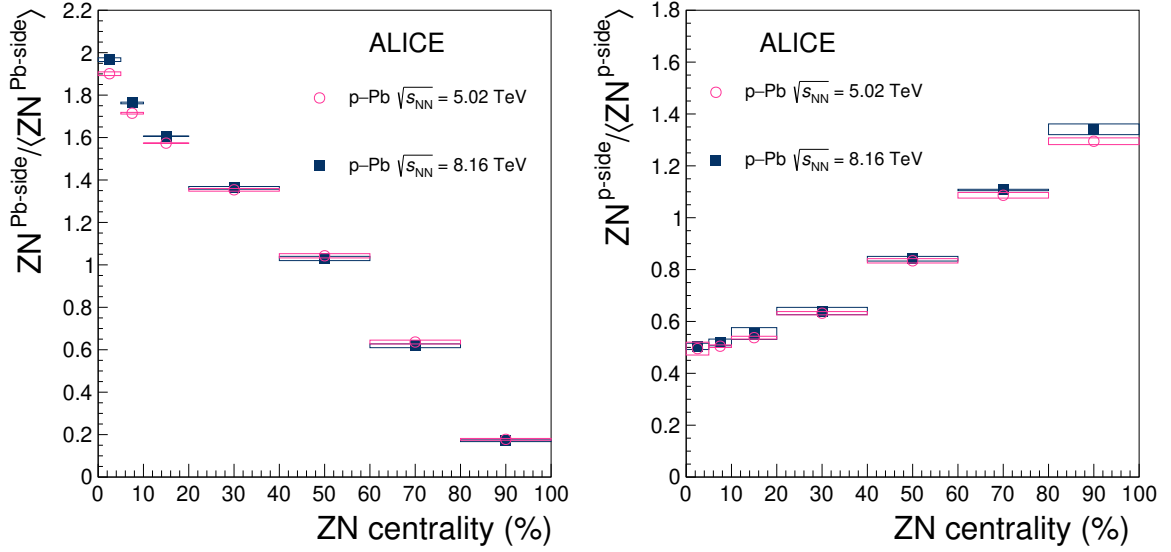


Figure 4: ZN energy normalised to the average MB value in the Pb-fragmentation (left) and in the p-fragmentation (right) regions as a function of centrality in p–Pb collisions at $\sqrt{s_{\text{NN}}} = 5.02$ TeV (pink circles) and 8.16 TeV (blue squares). The boxes represent the systematic uncertainty.

In Fig. 5, the normalised energies in the two fragmentation regions are shown as a function of the number of binary nucleon–nucleon collisions, N_{coll} , calculated as described in Ref. [13] and whose values are included in Ref. [24] for both p–Pb colliding energies. It is interesting to notice how the very forward energy in the p-fragmentation region is inversely dependent on centrality and on the number of binary collisions over a wide range of centralities.

5.2 Forward energy dependence on charged-particle multiplicity at midrapidity

The normalised ZN and ZP signals as a function of the charged-particle multiplicity measured at midrapidity in pp and in the p-fragmentation region in p–Pb collisions are compared in Fig. 6. In pp collisions the measurements performed with the ZDC on both p-fragmentation sides showed a compatible behaviour and their average has been computed. For p–Pb collisions two different data taking periods with inverted beam directions were averaged, being also in this case the A and C-side distributions compatible.

For pp collisions, two sources of systematic uncertainty were considered: the trigger selection and the difference between the measurements performed on both sides. The first contribution was estimated using a different trigger selection based on the AD detector, that removed some residual contribution due to single-diffractive events (estimated to be below 3‰ at 8 TeV[25]). This uncertainty ranged from 2% to 5% for ZN and from 2% to 6% for ZP. The uncertainty coming from considering the energy measured in two sides ranged from 0.3% to 1% for ZN and from 0.1% to 1% for ZP. The total uncertainty is calculated as the sum in quadrature of the two contributions and ranged from 2% to 5% for ZN and from 2% to 6% for ZP. In p–Pb collisions, the difference between the two beam configurations was considered as a source of systematic uncertainty and it ranged from 0.4% to 4% for ZN and 0.1% to 28% for ZP. The higher uncertainty values correspond to higher multiplicity bins, where the ZP signal is small, and this leads to a small absolute uncertainty value. The dependence of the detected forward energy on midrapidity multiplicity shows similar features in pp and in the p-fragmentation region in p–Pb collisions: the higher

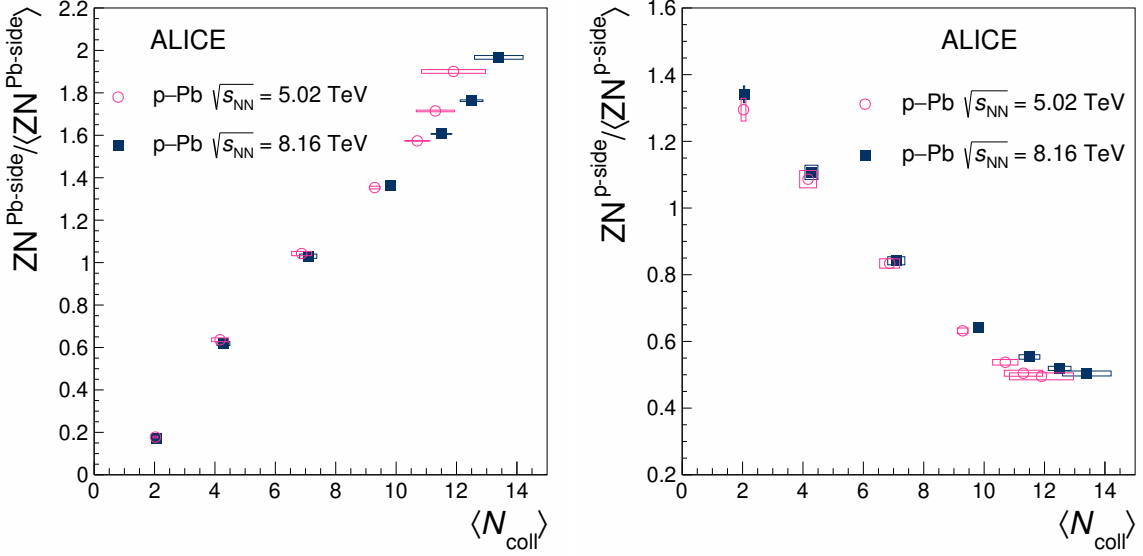


Figure 5: ZN energy normalised to the average MB value in the Pb-fragmentation (left) and in the p-fragmentation (right) regions as a function of the average N_{coll} in p–Pb collisions at $\sqrt{s_{\text{NN}}} = 5.02$ TeV (pink circles) and 8.16 TeV (blue squares). The boxes represent the systematic uncertainty.

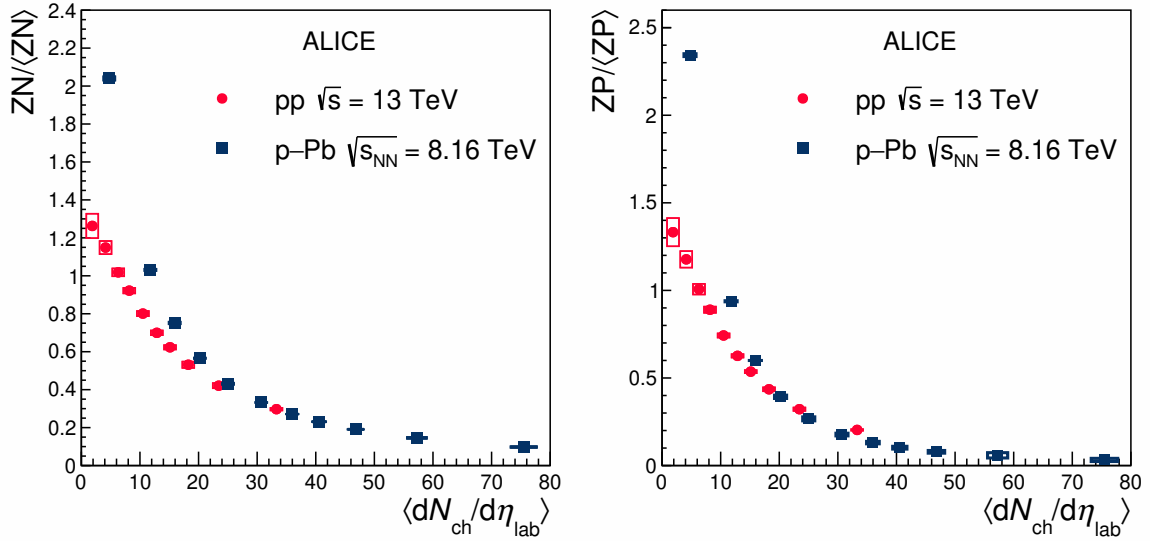


Figure 6: ZN (left) and ZP (right) self-normalised signals as a function of midrapidity multiplicity in pp (red circles) collisions and in the p-fragmentation region in p–Pb (blue squares) collisions. The boxes represent systematic uncertainties.

is the activity measured at midrapidity, the smaller is the forward energy.

The self-normalised forward energy as a function of the average multiplicity in a certain interval, normalised to the MB average, $\langle dN/d\eta \rangle / \langle dN/d\eta \rangle_{\text{MB}}$, was compared to MC simulations for pp collisions. All models are able to describe the overall decreasing trend, and PYTHIA 6 (Perugia 2011) is the one showing a higher degree of agreement, as is shown in Fig. 7. However, none of the models are able to reproduce the experimental results quantitatively. Moreover, they are not able to satisfactorily describe the measured forward energy spectra in multiplicity bins.

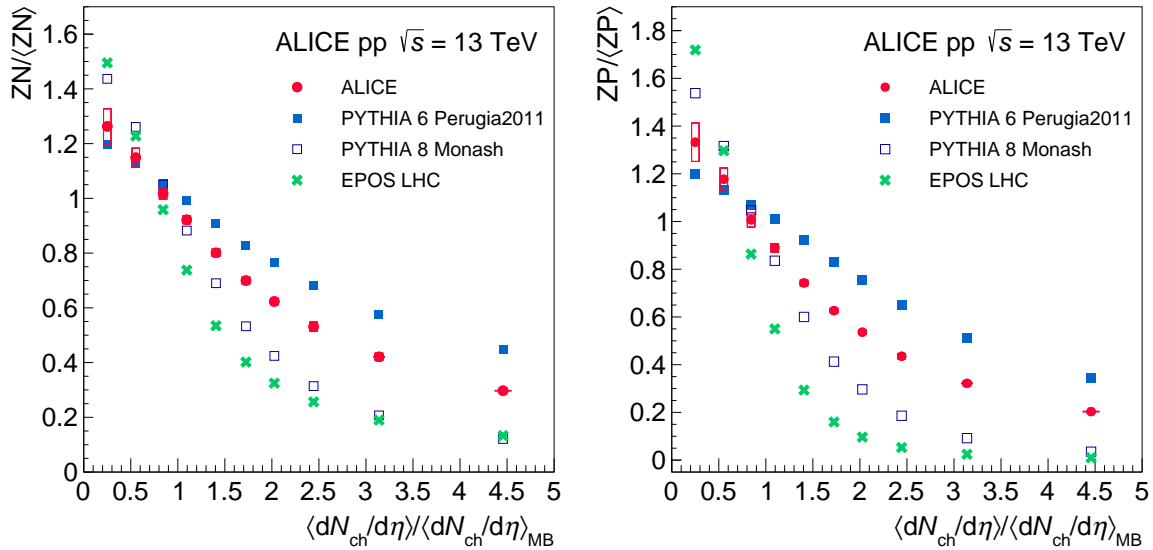


Figure 7: Self-normalised ZN (left) and ZP (right) signals as a function of the normalised charged-particle multiplicity produced in $|\eta| < 1$ in pp collisions. Data (red full circles) are compared to PYTHIA 6 (blue full squares), PYTHIA 8 (blue empty squares) and EPOS LHC (green crosses).

The PYTHIA event generator includes MPI modelling, which is needed to reproduce the energy flow measurements at LHC energies at smaller rapidities [26, 27]. The correlation between the very forward energy and the number of MPIs was studied using PYTHIA. Figure 8 shows the simulated ZN and ZP self-normalised responses as a function of the number of MPIs, normalised to their MB average value ($\langle N_{\text{MPI}} \rangle = 4.0$ for PYTHIA 6 Perugia 2011 and $\langle N_{\text{MPI}} \rangle = 5.0$ for PYTHIA 8 Monash). Both models predict a clear relationship between the very forward energy and N_{MPI} , showing a decrease in the average very forward energy for an increasing number of MPIs, albeit with different slopes due to the different treatment of MPIs in the two generators. This pattern resembles the observed dependence on charged-particle multiplicity (see Fig. 7), as can be expected in an impact-parameter dependent MPI picture [28].

The shape of the ZN spectrum also showed a dependence on the charged-particle multiplicity at midrapidity. To characterise these modifications, three narrow multiplicity intervals were selected, corresponding to high (0–2%), intermediate (20–30%) and low (50–80%) multiplicities, and the ZN spectrum was compared to the MB distribution in these intervals. Figure 9 shows the spectrum modifications in the considered multiplicity intervals. In particular, as predicted in Refs. [22, 29], the forward leading neutron energy is suppressed when a higher activity is measured at midrapidity.

5.3 Correlation between forward energy and leading particle transverse momentum

The forward energy was studied as a function of the leading particle transverse momentum, $p_{\text{T}}^{\text{leading}}$, defined event by event as the track with the largest transverse momentum in $|\eta| < 0.8$. Events with large forward energies are characterised by smaller values of the leading particle p_{T} , as already observed in measurements at smaller pseudorapidities at the LHC [30]. The self-normalised ZN and ZP signals as a function of the leading particle p_{T} are shown in Fig. 10. The total systematic uncertainty was estimated as the sum in quadrature of three contributions: the first one coming from the trigger selection, the second due to the differences between the measurements performed on the two sides, and the third contribution takes into account the misidentification of the leading particle that is corrected for with a data-driven procedure, as detailed in Ref. [31]. The total uncertainty ranges from 0.8% to 4.4% for ZN and from 0.8% to 5.5% for ZP, the dominant contribution coming from the difference between the two sides. A

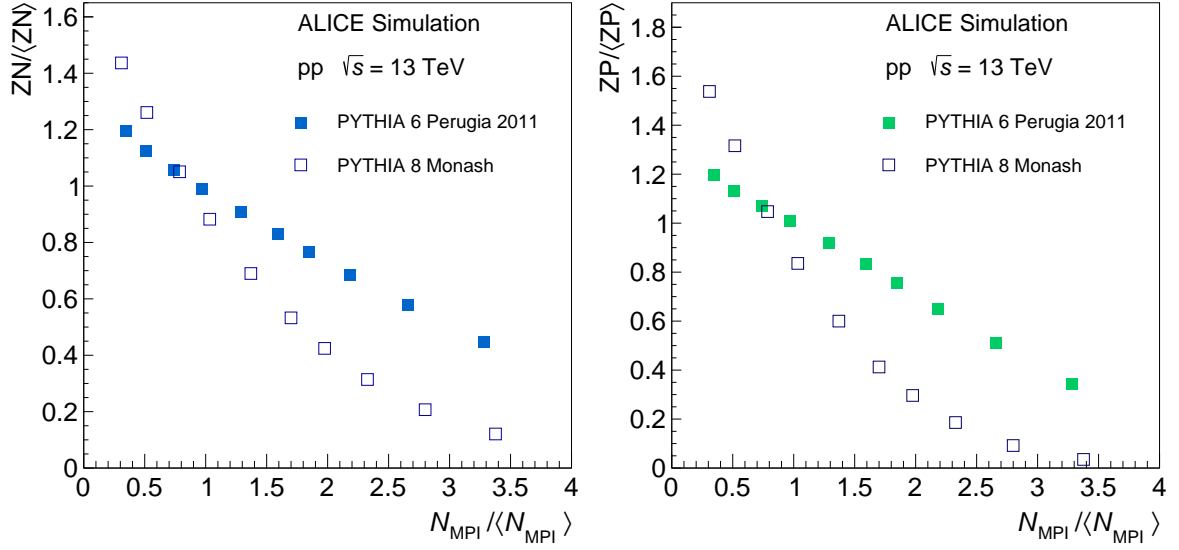


Figure 8: Self-normalised ZN (left) and ZP (right) signal as a function of the number of self-normalised MPI extracted from PYTHIA 6 Perugia 2011 (full squares) and PYTHIA 8 Monash (empty squares) tunes.

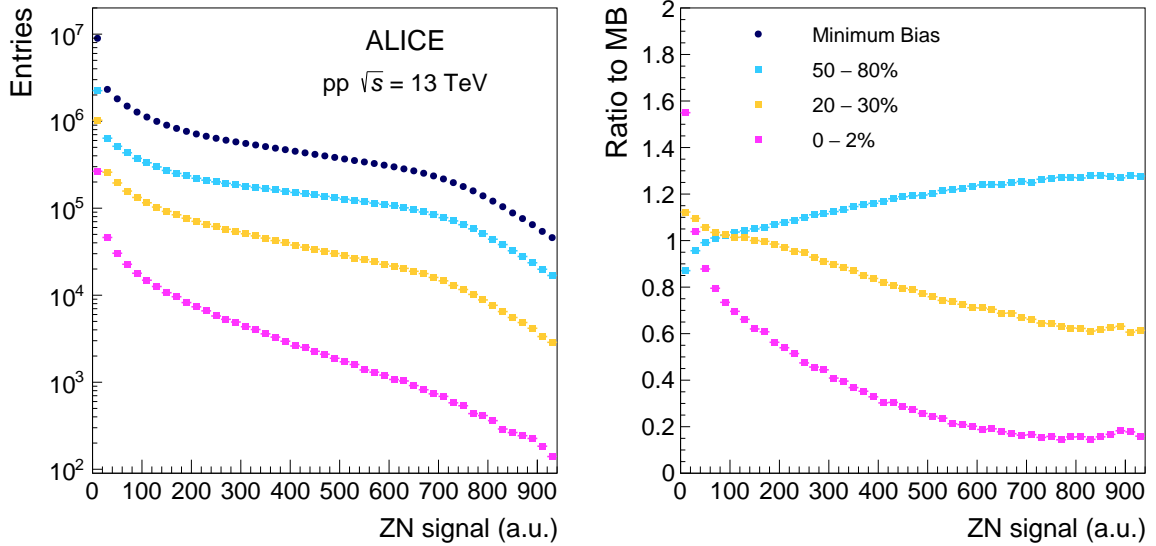


Figure 9: Left: ZN spectrum in pp collisions at $\sqrt{s}=13$ TeV for the MB sample (blue circles) and in three multiplicity intervals: high (magenta squares), intermediate (orange squares) and low (azure squares) multiplicity. Right: ratio of the spectra, normalised to the number of events in each bin, in the three multiplicity intervals to the MB spectrum.

large forward energy is measured for very low values of the leading particle p_T ($p_T^{\text{leading}} < 1$ GeV/c). For larger leading particle p_T values, ZN and ZP energies rapidly decrease and saturate for $p_T^{\text{leading}} \gtrsim 5$ GeV/c. The same trend was reported by the CMS collaboration when measuring the energy at smaller rapidities ($-6.6 < \eta < -5.2$) [26].

The self-normalised ZN and ZP signals as a function of the leading particle p_T are also compared in Fig. 10 to the three models under consideration. The trend predicted by PYTHIA 6 is qualitatively in agreement with data, even if, for a leading particle p_T larger than 2 GeV/c, PYTHIA 6 overestimates

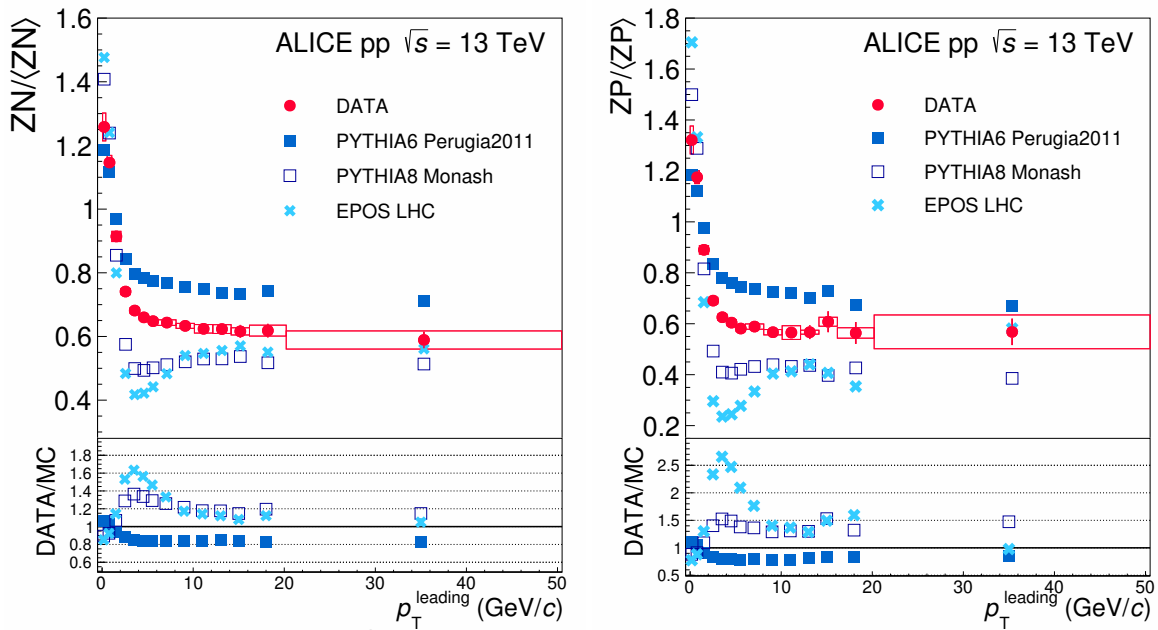


Figure 10: Self-normalised ZN (left) and ZP (right) signals as a function of the leading particle p_T measured in $|\eta| < 0.8$ in pp collisions at $\sqrt{s} = 13$ TeV. Data (red full circles) are compared to PYTHIA 6 (blue full squares), PYTHIA 8 (blue empty squares) and EPOS LHC (azure crosses).

the forward energy by almost 20%. On the contrary, the leading particle p_T dependence predicted by PYTHIA 8 is different for intermediate p_T values (2–8 GeV/c). This seems to indicate that the treatment of colour reconnections and beam remnants in the Perugia tunes of PYTHIA 6 is more realistic than the one in the default Monash tune of PYTHIA 8. The core–corona EPOS LHC event generator also predicts a quite different pattern, in particular it shows a depletion for intermediate p_T values (2–8 GeV/c), where collective expansion (flow) included in the core part of the model might play a major role.

5.4 Very forward energy and event properties in pp collisions

The energy carried forward by leading baryons has been proposed as a tool to select events with smaller than average impact parameter. In Ref. [6] a double veto on leading baryon production is suggested as an effective way to select events characterised by a narrower impact-parameter distribution and harder particle spectra. To test this hypothesis, the energy detected by the ZDC was used as a veto, requesting that neither ZN nor ZP have a signal on one or on both sides, defining thus a single-side and a double-side veto condition on leading baryon production, respectively. The charged-particle multiplicity in $|\eta| < 1$ and the total transverse momentum in $|\eta| < 0.8$ were compared applying these conditions. The charged particle distributions are corrected using MC simulations with different generators, and the systematic uncertainty is estimated using EPOS LHC and Pythia 8. The correction factors for the total p_T distributions, to account for tracking efficiency and secondary contamination, were extracted from [32], and the systematic uncertainty is estimated varying the p_T within the obtained boundaries. The distributions are corrected only for inefficiencies and not for effects related to resolution. However, they provide a clear indication of the effect due to the different applied conditions. In Fig. 11, N_{ch} and p_T^{TOT} distributions for the MB and for the two vetoed samples are shown. The average values of N_{ch} are a factor ~ 1.2 and ~ 1.5 higher than in the MB sample for the single and double veto selection, respectively. The analysis of the simulated samples provided similar results, yielding to similar increases for the average values of N_{ch} , namely a factor (1.1) 1.3 for PYTHIA 6, (1.2) 1.6 for to PYTHIA 8 and (1.2) 1.4 using EPOS LHC, applying the (single) double veto condition. In conclusion, a double-side veto condition selects a larger than average multiplicity and a harder p_T distribution at midrapidity. This measurement supports the pre-

diction that a double side veto on baryon production leads to a narrower impact-parameter distribution.

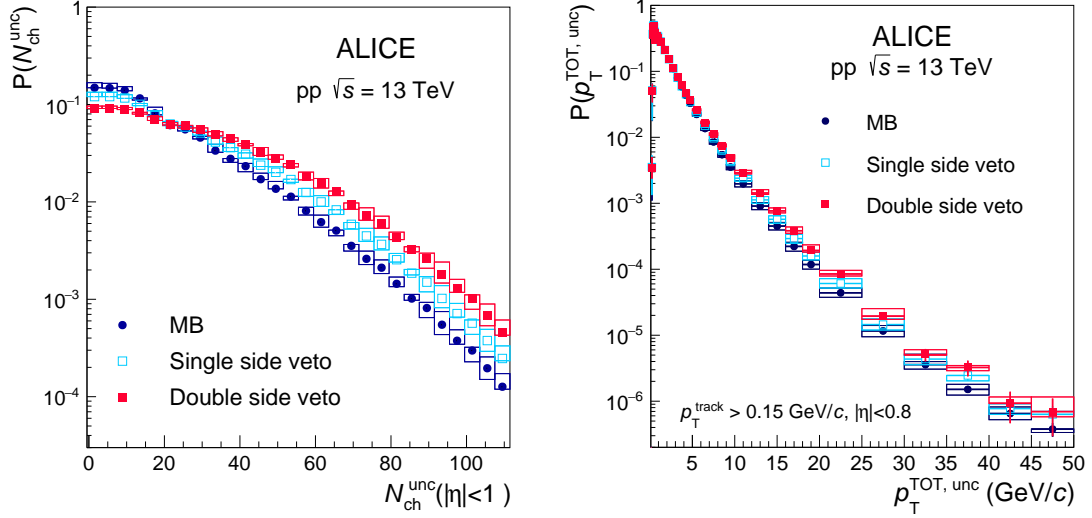


Figure 11: Distributions of the (not fully corrected) number of charged particles in $|\eta| < 1$ (left) and of the total transverse momentum in $|\eta| < 0.8$ (right) for MB interactions (blue circles), single-side (azure empty squares) and double-side (red full squares) veto conditions on leading baryon production in pp collisions at $\sqrt{s} = 13$ TeV.

The measurement of the forward energy as a function of the leading particle p_T measured at midrapidity is complementary to the UE, defined through the charged-particle multiplicity produced in the azimuthal region transverse to the emitted leading particle ($60^\circ < |\Delta\phi| < 120^\circ$) [31]. The charged-particle multiplicity in the transverse region rapidly reaches its maximum value and then remains constant for increasing p_T (pedestal effect), while the forward energy (both for neutrons and protons) reaches its minimum value and then remains constant for increasing particle p_T at midrapidity. These two saturation effects occur at the same leading particle p_T scale, around $p_T \sim 5$ GeV/c, as can be seen in Fig. 12, where UE published results [32] and ZN normalised energy are compared for pp collisions at $\sqrt{s} = 13$ TeV. In the MPI approach, collisions producing high- p_T particles have a lower than average impact parameter and consequently a larger underlying event activity [23]. Above a leading particle p_T of about 5 GeV/c the impact parameter bias reaches its maximum value. The strong anti-correlation between the leading particle p_T and the forward energy seen at low p_T^{leading} can only be built in the initial stages of the collisions, since the two observables are causally disconnected in the following evolution stages.

6 Conclusions

First results on the very forward energy measured by the ALICE ZDC in pp collisions at $\sqrt{s} = 13$ TeV and in p–Pb collisions at $\sqrt{s_{NN}} = 8.16$ TeV have been presented.

In pp collisions, the energy carried by leading protons at large forward and backward rapidities is found to be uncorrelated, confirming results from hadronic collisions at lower energies, while for neutrons a weak correlation between the energy released at forward and backward rapidities is observed.

The very forward energy was studied as a function of the charged-particle production at midrapidity to gain insight in the particle production mechanisms. The self-normalised forward energy decreases with increasing charged-particle multiplicity at midrapidity, both in pp and in p–Pb collisions with the same proton beam energy.

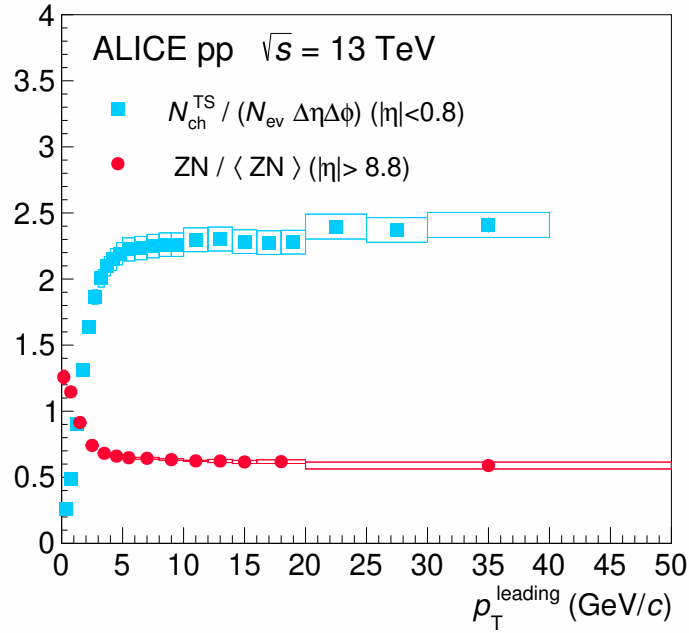


Figure 12: Self-normalised ZN signal (red circles) and number density N_{ch} (azure squares) distribution in the transverse region (published in Ref. [32]) as a function of p_T^{leading} measured in $|\eta| < 0.8$. Tracks have $p_T > 0.15$ GeV/c, markers are placed at the centre and not at the average of the p_T leading bin.

The very forward energy decreases with increasing leading particle p_T at midrapidity until about 5 GeV/c where it saturates. Similarly, the charged-particle multiplicity in the transverse region (UE) as a function of the leading particle p_T first rises and then saturates at about the same p_T . In the case of the UE this is commonly interpreted as a bias to an on average smaller pp impact parameter with consequently larger number of MPIs leading to higher multiplicity at midrapidity. The results of this paper corroborate this interpretation since the correlation between central and forward rapidity can only be attributed to the initial stage of the collisions.

The hadronic interaction models used for comparison, PYTHIA 6 Perugia 2011, PYTHIA 8 Monash, and EPOS-LHC, are not able to reproduce quantitatively the measurements at large rapidities as a function of particle production at midrapidity. These measurements provide constraints to improve the model description of beam remnants and very forward energy.

Finally, it was shown that the very forward energy can be effectively used in pp collisions as a veto to select events characterised by higher than total average multiplicity and total transverse momentum, in agreement with expectations from models including centrality dependent particle production.

Acknowledgements

The ALICE Collaboration would like to thank all its engineers and technicians for their invaluable contributions to the construction of the experiment and the CERN accelerator teams for the outstanding performance of the LHC complex. The ALICE Collaboration gratefully acknowledges the resources and support provided by all Grid centres and the Worldwide LHC Computing Grid (WLCG) collaboration. The ALICE Collaboration acknowledges the following funding agencies for their support in building and running the ALICE detector: A. I. Alikhanyan National Science Laboratory (Yerevan Physics Institute) Foundation (ANSL), State Committee of Science and World Federation of Scientists (WFS), Armenia; Austrian Academy of Sciences, Austrian Science Fund (FWF): [M 2467-N36] and Nationalstiftung für Forschung, Technologie und Entwicklung, Austria; Ministry of Communications and High

Technologies, National Nuclear Research Center, Azerbaijan; Conselho Nacional de Desenvolvimento Científico e Tecnológico (CNPq), Financiadora de Estudos e Projetos (Finep), Fundação de Amparo à Pesquisa do Estado de São Paulo (FAPESP) and Universidade Federal do Rio Grande do Sul (UFRGS), Brazil; Ministry of Education of China (MOEC), Ministry of Science & Technology of China (MSTC) and National Natural Science Foundation of China (NSFC), China; Ministry of Science and Education and Croatian Science Foundation, Croatia; Centro de Aplicaciones Tecnológicas y Desarrollo Nuclear (CEADEN), Cubaenergía, Cuba; Ministry of Education, Youth and Sports of the Czech Republic, Czech Republic; The Danish Council for Independent Research | Natural Sciences, the VILLUM FONDEN and Danish National Research Foundation (DNRF), Denmark; Helsinki Institute of Physics (HIP), Finland; Commissariat à l’Energie Atomique (CEA) and Institut National de Physique Nucléaire et de Physique des Particules (IN2P3) and Centre National de la Recherche Scientifique (CNRS), France; Bundesministerium für Bildung und Forschung (BMBF) and GSI Helmholtzzentrum für Schwerionenforschung GmbH, Germany; General Secretariat for Research and Technology, Ministry of Education, Research and Religions, Greece; National Research, Development and Innovation Office, Hungary; Department of Atomic Energy Government of India (DAE), Department of Science and Technology, Government of India (DST), University Grants Commission, Government of India (UGC) and Council of Scientific and Industrial Research (CSIR), India; Indonesian Institute of Science, Indonesia; Istituto Nazionale di Fisica Nucleare (INFN), Italy; Institute for Innovative Science and Technology, Nagasaki Institute of Applied Science (IIST), Japanese Ministry of Education, Culture, Sports, Science and Technology (MEXT) and Japan Society for the Promotion of Science (JSPS) KAKENHI, Japan; Consejo Nacional de Ciencia (CONACYT) y Tecnología, through Fondo de Cooperación Internacional en Ciencia y Tecnología (FONCICYT) and Dirección General de Asuntos del Personal Académico (DGAPA), Mexico; Nederlandse Organisatie voor Wetenschappelijk Onderzoek (NWO), Netherlands; The Research Council of Norway, Norway; Commission on Science and Technology for Sustainable Development in the South (COMSATS), Pakistan; Pontificia Universidad Católica del Perú, Peru; Ministry of Education and Science, National Science Centre and WUT ID-UB, Poland; Korea Institute of Science and Technology Information and National Research Foundation of Korea (NRF), Republic of Korea; Ministry of Education and Scientific Research, Institute of Atomic Physics and Ministry of Research and Innovation and Institute of Atomic Physics, Romania; Joint Institute for Nuclear Research (JINR), Ministry of Education and Science of the Russian Federation, National Research Centre Kurchatov Institute, Russian Science Foundation and Russian Foundation for Basic Research, Russia; Ministry of Education, Science, Research and Sport of the Slovak Republic, Slovakia; National Research Foundation of South Africa, South Africa; Swedish Research Council (VR) and Knut & Alice Wallenberg Foundation (KAW), Sweden; European Organization for Nuclear Research, Switzerland; Suranaree University of Technology (SUT), National Science and Technology Development Agency (NSDTA) and Office of the Higher Education Commission under NRU project of Thailand, Thailand; Turkish Energy, Nuclear and Mineral Research Agency (TENMAK), Turkey; National Academy of Sciences of Ukraine, Ukraine; Science and Technology Facilities Council (STFC), United Kingdom; National Science Foundation of the United States of America (NSF) and United States Department of Energy, Office of Nuclear Physics (DOE NP), United States of America.

References

- [1] CMS Collaboration, V. Khachatryan *et al.*, “Evidence for collectivity in pp collisions at the LHC,” *Phys. Lett. B* **765** (2017) 193–220, arXiv:1606.06198 [nucl-ex].
- [2] ALICE Collaboration, B. Abelev *et al.*, “Long-range angular correlations on the near and away side in p–Pb collisions at $\sqrt{s_{NN}} = 5.02$ TeV,” *Phys. Lett. B* **719** (2013) 29–41, arXiv:1212.2001 [nucl-ex].

- [3] ALICE Collaboration, J. Adam *et al.*, “Enhanced production of multi-strange hadrons in high-multiplicity proton-proton collisions,” *Nature Phys.* **13** (2017) 535–539, arXiv:1606.07424 [nucl-ex].
- [4] ALICE Collaboration, J. Adam *et al.*, “Pseudorapidity and transverse-momentum distributions of charged particles in proton–proton collisions at $\sqrt{s} = 13$ TeV,” *Phys. Lett. B* **753** (2016) 319–329, arXiv:1509.08734 [nucl-ex].
- [5] T. Pierog, “Hadronic Interactions and Air Showers: Where Do We Stand?,” *EPJ Web Conf.* **208** (2019) 02002.
- [6] H. J. Drescher and M. Strikman, “How to probe high gluon densities in p p collisions at the Large Hadron Collider,” *Phys. Rev. Lett.* **100** (2008) 152002.
- [7] ALICE Collaboration, K. Aamodt *et al.*, “The ALICE experiment at the CERN LHC,” *JINST* **3** (2008) S08002.
- [8] ALICE Collaboration, B. B. Abelev *et al.*, “Performance of the ALICE Experiment at the CERN LHC,” *Int. J. Mod. Phys. A* **29** (2014) 1430044, arXiv:1402.4476 [nucl-ex].
- [9] J. Alme *et al.*, “The ALICE TPC, a large 3-dimensional tracking device with fast readout for ultra-high multiplicity events,” *Nucl. Instrum. Meth. A* **622** (2010) 316–367, arXiv:1001.1950 [physics.ins-det].
- [10] ALICE Collaboration, E. Abbas *et al.*, “Performance of the ALICE VZERO system,” *JINST* **8** (2013) P10016, arXiv:1306.3130 [nucl-ex].
- [11] M. Broz *et al.*, “Performance of ALICE AD modules in the CERN PS test beam,” *JINST* **16** no. 01, (2021) P01017, arXiv:2006.14982 [physics.ins-det].
- [12] ALICE Collaboration, B. Abelev *et al.*, “Centrality determination of Pb-Pb collisions at $\sqrt{s_{NN}} = 2.76$ TeV with ALICE,” *Phys. Rev. C* **88** no. 4, (2013) 044909, arXiv:1301.4361 [nucl-ex].
- [13] ALICE Collaboration, J. Adam *et al.*, “Centrality dependence of particle production in p-Pb collisions at $\sqrt{s_{NN}} = 5.02$ TeV,” *Phys. Rev. C* **91** no. 6, (2015) 064905, arXiv:1412.6828 [nucl-ex].
- [14] ALICE Collaboration, S. Acharya *et al.*, “Pseudorapidity distributions of charged particles as a function of mid and forward rapidity multiplicities in pp collisions at $\sqrt{s} = 5.02, 7$ and 13 TeV,” arXiv:2009.09434 [nucl-ex].
- [15] ALICE Collaboration, S. Acharya *et al.*, “Charged-particle pseudorapidity density at mid-rapidity in p-Pb collisions at $\sqrt{s_{NN}} = 8.16$ TeV,” *Eur. Phys. J. C* **79** no. 4, (2019) 307, arXiv:1812.01312 [nucl-ex].
- [16] P. Skands, “Tuning Monte Carlo Generators: The Perugia Tunes,” *Phys. Rev. D* **82** (2010) 074018, arXiv:1005.3457 [hep-ph].
- [17] P. Skands, S. Carrazza, and J. Rojo, “Tuning PYTHIA 8.1: the Monash 2013 Tune,” *Eur. Phys. J. C* **74** no. 8, (2014) 3024, arXiv:1404.5630 [hep-ph].
- [18] T. Pierog, I. Karpenko, J. M. Katzy, E. Yatsenko, and K. Werner, “EPOS LHC: Test of collective hadronization with data measured at the CERN Large Hadron Collider,” *Phys. Rev. C* **92** no. 3, (2015) 034906, arXiv:1306.0121 [hep-ph].

- [19] R. Brun, F. Bruyant, F. Carminati, S. Giani, M. Maire, A. McPherson, G. Patrick, and L. Urban, *GEANT: Detector Description and Simulation Tool; Oct 1994*. CERN Program Library. CERN, Geneva, 1993. <https://cds.cern.ch/record/1082634>. Long Writeup W5013.
- [20] M. Basile *et al.*, “Experimental Proof That the Leading Protons Are Not Correlated,” *Nuovo Cim. A* **73** (1983) 329.
- [21] L. Frankfurt, M. Strikman, and C. Weiss, “Transverse nucleon structure and diagnostics of hard parton-parton processes at LHC,” *Phys. Rev. D* **83** (2011) 054012, arXiv:1009.2559 [hep-ph].
- [22] H. J. Drescher and M. Strikman, “Toward an effective centrality trigger in pp collisions at LHC,” arXiv:0712.3209 [hep-ph].
- [23] T. Martin, P. Skands, and S. Farrington, “Probing Collective Effects in Hadronisation with the Extremes of the Underlying Event,” *Eur. Phys. J. C* **76** no. 5, (2016) 299, arXiv:1603.05298 [hep-ph].
- [24] ALICE Collaboration, S. Acharya *et al.*, “Centrality determination in heavy ion collisions,” *ALICE-PUBLIC-2018-011* (Aug, 2018). <https://cds.cern.ch/record/2636623>.
- [25] ALICE Collaboration, J. Adam *et al.*, “Charged-particle multiplicities in proton–proton collisions at $\sqrt{s} = 0.9$ to 8 TeV,” *Eur. Phys. J. C* **77** no. 1, (2017) 33, arXiv:1509.07541 [nucl-ex].
- [26] CMS Collaboration, S. Chatrchyan *et al.*, “Study of the Underlying Event at Forward Rapidity in pp Collisions at $\sqrt{s} = 0.9, 2.76,$ and 7 TeV,” *JHEP* **04** (2013) 072, arXiv:1302.2394 [hep-ex].
- [27] CMS Collaboration, S. Chatrchyan *et al.*, “Measurement of energy flow at large pseudorapidities in pp collisions at $\sqrt{s} = 0.9$ and 7 TeV,” *JHEP* **11** (2011) 148, arXiv:1110.0211 [hep-ex]. [Erratum: *JHEP* 02, 055 (2012)].
- [28] T. Sjöstrand, “The Development of MPI Modeling in Pythia,” *Adv. Ser. Direct. High Energy Phys.* **29** (2018) 191–225, arXiv:1706.02166 [hep-ph].
- [29] A. Dumitru, L. Gerland, and M. Strikman, “Proton breakup in high-energy pA collisions from perturbative QCD,” *Phys. Rev. Lett.* **90** (2003) 092301, arXiv:hep-ph/0211324. [Erratum: *Phys.Rev.Lett.* 91, 259901 (2003)].
- [30] ATLAS Collaboration, G. Aad *et al.*, “Measurement of the dependence of transverse energy production at large pseudorapidity on the hard-scattering kinematics of proton-proton collisions at $\sqrt{s} = 2.76$ TeV with ATLAS,” *Phys. Lett. B* **756** (2016) 10–28, arXiv:1512.00197 [hep-ex].
- [31] ALICE Collaboration, B. Abelev *et al.*, “Underlying Event measurements in pp collisions at $\sqrt{s} = 0.9$ and 7 TeV with the ALICE experiment at the LHC,” *JHEP* **07** (2012) 116, arXiv:1112.2082 [hep-ex].
- [32] ALICE Collaboration, S. Acharya *et al.*, “Underlying Event properties in pp collisions at $\sqrt{s} = 13$ TeV,” *JHEP* **04** (2020) 192, arXiv:1910.14400 [nucl-ex].

A The ALICE Collaboration

S. Acharya¹⁴³, D. Adamová⁹⁸, A. Adler⁷⁶, G. Aglieri Rinella³⁵, M. Agnello³¹, N. Agrawal⁵⁵, Z. Ahammed¹⁴³, S. Ahmad¹⁶, S.U. Ahn⁷⁸, I. Ahuja³⁹, Z. Akbar⁵², A. Akindinov⁹⁵, M. Al-Turany¹¹⁰, S.N. Alam^{16,41}, D. Aleksandrov⁹¹, B. Alessandro⁶¹, H.M. Alfanda⁷, R. Alfaro Molina⁷³, B. Ali¹⁶, Y. Ali¹⁴, A. Alici²⁶, N. Alizadehvandchali¹²⁷, A. Alkin³⁵, J. Alme²¹, T. Alt⁷⁰, L. Altenkamper²¹, I. Altsybeev¹¹⁵, M.N. Anaam⁷, C. Andrei⁴⁹, D. Andreou⁹³, A. Andronic¹⁴⁶, M. Angeletti³⁵, V. Anguelov¹⁰⁷, F. Antinori⁵⁸, P. Antonioli⁵⁵, C. Anuj¹⁶, N. Apadula⁸², L. Aphecetche¹¹⁷, H. Appelshäuser⁷⁰, S. Arcelli²⁶, R. Arnaldi⁶¹, I.C. Arsene²⁰, M. Arslandok^{148,107}, A. Augustinus³⁵, R. Averbeck¹¹⁰, S. Aziz⁸⁰, M.D. Azmi¹⁶, A. Badalá⁵⁷, Y.W. Baek⁴², X. Bai^{131,110}, R. Bailhache⁷⁰, Y. Bailung⁵¹, R. Bala¹⁰⁴, A. Balbino³¹, A. Baldisseri¹⁴⁰, B. Balis², M. Ball⁴⁴, D. Banerjee⁴, R. Barbera²⁷, L. Barioglio¹⁰⁸, M. Barlou⁸⁷, G.G. Barnaföldi¹⁴⁷, L.S. Barnby⁹⁷, V. Barret¹³⁷, C. Bartels¹³⁰, K. Barth³⁵, E. Bartsch⁷⁰, F. Baruffaldi²⁸, N. Bastid¹³⁷, S. Basu⁸³, G. Batigne¹¹⁷, B. Batyunya⁷⁷, D. Bauri⁵⁰, J.L. Bazo Alba¹¹⁴, I.G. Bearden⁹², C. Beattie¹⁴⁸, I. Belikov¹³⁹, A.D.C. Bell Hechavarria¹⁴⁶, F. Bellini²⁶, R. Bellwied¹²⁷, S. Belokurova¹¹⁵, V. Belyaev⁹⁶, G. Bencedi⁷¹, S. Beole²⁵, A. Bercuci⁴⁹, Y. Berdnikov¹⁰¹, A. Berdnikova¹⁰⁷, L. Bergmann¹⁰⁷, M.G. Besoiu⁶⁹, L. Betev³⁵, P.P. Bhaduri¹⁴³, A. Bhasin¹⁰⁴, I.R. Bhat¹⁰⁴, M.A. Bhat⁴, B. Bhattacharjee⁴³, P. Bhattacharya²³, L. Bianchi²⁵, N. Bianchi⁵³, J. Bielčik³⁸, J. Bielčiková⁹⁸, J. Biernat¹²⁰, A. Bilandžić¹⁰⁸, G. Biro¹⁴⁷, S. Biswas⁴, J.T. Blair¹²¹, D. Blau⁹¹, M.B. Blidaru¹¹⁰, C. Blume⁷⁰, G. Boca^{29,59}, F. Bock⁹⁹, A. Bogdanov⁹⁶, S. Boi²³, J. Bok⁶³, L. Boldizsár¹⁴⁷, A. Bolozdynya⁹⁶, M. Bombara³⁹, P.M. Bond³⁵, G. Bonomi^{142,59}, H. Borel¹⁴⁰, A. Borissov⁸⁴, H. Bossi¹⁴⁸, E. Botta²⁵, L. Bratrud⁷⁰, P. Braun-Munzinger¹¹⁰, M. Bregant¹²³, M. Broz³⁸, G.E. Bruno^{109,34}, M.D. Buckland¹³⁰, D. Budnikov¹¹¹, H. Buesching⁷⁰, S. Bufalino³¹, O. Bugnon¹¹⁷, P. Buhler¹¹⁶, Z. Buthelezi^{74,134}, J.B. Butt¹⁴, S.A. Bysiak¹²⁰, M. Cai^{28,7}, H. Caines¹⁴⁸, A. Caliva¹¹⁰, E. Calvo Villar¹¹⁴, J.M.M. Camacho¹²², R.S. Camacho⁴⁶, P. Camerini²⁴, F.D.M. Canedo¹²³, F. Carnesecchi^{35,26}, R. Caron¹⁴⁰, J. Castillo Castellanos¹⁴⁰, E.A.R. Casula²³, F. Catalano³¹, C. Ceballos Sanchez⁷⁷, P. Chakraborty⁵⁰, S. Chandra¹⁴³, S. Chapeland³⁵, M. Chartier¹³⁰, S. Chattopadhyay¹⁴³, S. Chattopadhyay¹¹², A. Chauvin²³, T.G. Chavez⁴⁶, T. Cheng⁷, C. Cheshkov¹³⁸, B. Cheynis¹³⁸, V. Chibante Barroso³⁵, D.D. Chinellato¹²⁴, S. Cho⁶³, P. Chochula³⁵, P. Christakoglou⁹³, C.H. Christensen⁹², P. Christiansen⁸³, T. Chujo¹³⁶, C. Cicalo⁵⁶, L. Cifarelli²⁶, F. Cindolo⁵⁵, M.R. Ciupek¹¹⁰, G. Clai^{II,55}, J. Cleymans^{I,126}, F. Colamaria⁵⁴, J.S. Colburn¹¹³, D. Colella^{109,54,34,147}, A. Collu⁸², M. Colocci³⁵, M. Concas^{III,61}, G. Conesa Balbastre⁸¹, Z. Conesa del Valle⁸⁰, G. Contin²⁴, J.G. Contreras³⁸, M.L. Coquet¹⁴⁰, T.M. Cormier⁹⁹, P. Cortese³², M.R. Cosentino¹²⁵, F. Costa³⁵, S. Costanza^{29,59}, P. Crochet¹³⁷, R. Cruz-Torres⁸², E. Cuautle⁷¹, P. Cui⁷, L. Cunqueiro⁹⁹, A. Dainese⁵⁸, M.C. Danisch¹⁰⁷, A. Danu⁶⁹, I. Das¹¹², P. Das⁸⁹, P. Das⁴, S. Das⁴, S. Dash⁵⁰, S. De⁸⁹, A. De Caro³⁰, G. de Cataldo⁵⁴, L. De Cilladi²⁵, J. de Cuveland⁴⁰, A. De Falco²³, D. De Gruttola³⁰, N. De Marco⁶¹, C. De Martin²⁴, S. De Pasquale³⁰, S. Deb⁵¹, H.F. Degenhardt¹²³, K.R. Deja¹⁴⁴, L. Dello Stritto³⁰, S. Delsanto²⁵, W. Deng⁷, P. Dhankher¹⁹, D. Di Bari³⁴, A. Di Mauro³⁵, R.A. Diaz⁸, T. Dietel¹²⁶, Y. Ding^{138,7}, R. Divià³⁵, D.U. Dixit¹⁹, Ø. Djuvsland²¹, U. Dmitrieva⁶⁵, J. Do⁶³, A. Dobrin⁶⁹, B. Dönigus⁷⁰, O. Dordic²⁰, A.K. Dubey¹⁴³, A. Dubla^{110,93}, S. Dudi¹⁰³, M. Dukhishyam⁸⁹, P. Dupieux¹³⁷, N. Dzalaiova¹³, T.M. Eder¹⁴⁶, R.J. Ehlers⁹⁹, V.N. Eikeland²¹, F. Eisenhut⁷⁰, D. Elia⁵⁴, B. Erasmus¹¹⁷, F. Ercolessi²⁶, F. Erhardt¹⁰², A. Erokhin¹¹⁵, M.R. Ersdal²¹, B. Espagnon⁸⁰, G. Eulisse³⁵, D. Evans¹¹³, S. Evdokimov⁹⁴, L. Fabbietti¹⁰⁸, M. Faggin²⁸, J. Faivre⁸¹, F. Fan⁷, A. Fantoni⁵³, M. Fasel⁹⁹, P. Fedichio³¹, A. Feliciello⁶¹, G. Feofilov¹¹⁵, A. Fernández Téllez⁴⁶, A. Ferrero¹⁴⁰, A. Ferretti²⁵, V.J.G. Feuillard¹⁰⁷, J. Figiel¹²⁰, S. Filchagin¹¹¹, D. Finogeev⁶⁵, F.M. Fionda^{56,21}, G. Fiorenza^{35,109}, F. Flor¹²⁷, A.N. Flores¹²¹, S. Foertsch⁷⁴, P. Foka¹¹⁰, S. Fokin⁹¹, E. Fragiaco⁶², E. Frajna¹⁴⁷, U. Fuchs³⁵, N. Funicello³⁰, C. Furget⁸¹, A. Furs⁶⁵, J.J. Gaardhøje⁹², M. Gagliardi²⁵, A.M. Gago¹¹⁴, A. Gal¹³⁹, C.D. Galvan¹²², P. Ganoti⁸⁷, C. Garabatos¹¹⁰, J.R.A. Garcia⁴⁶, E. Garcia-Solis¹⁰, K. Garg¹¹⁷, C. Gargiulo³⁵, A. Garibli⁹⁰, K. Garner¹⁴⁶, P. Gasik¹¹⁰, E.F. Gauger¹²¹, A. Gautam¹²⁹, M.B. Gay Ducati⁷², M. Germain¹¹⁷, P. Ghosh¹⁴³, S.K. Ghosh⁴, M. Giacalone²⁶, P. Gianotti⁵³, P. Giubellino^{110,61}, P. Giubilato²⁸, A.M.C. Glaenger¹⁴⁰, P. Glässel¹⁰⁷, D.J.Q. Goh⁸⁵, V. Gonzalez¹⁴⁵, L.H. González-Trueba⁷³, S. Gorbunov⁴⁰, M. Gorgon², L. Görlich¹²⁰, S. Gotovac³⁶, V. Grabski⁷³, L.K. Graczykowski¹⁴⁴, L. Greiner⁸², A. Grelli⁶⁴, C. Grigoras³⁵, V. Grigoriev⁹⁶, A. Grigoryan^{I,1}, S. Grigoryan^{77,1}, O.S. Groettvik²¹, F. Grosa^{35,61}, J.F. Grosse-Oetringhaus³⁵, R. Grosso¹¹⁰, G.G. Guardiano¹²⁴, R. Guernane⁸¹, M. Guilbaud¹¹⁷, K. Gulbrandsen⁹², T. Gunji¹³⁵, W. Guo⁷, A. Gupta¹⁰⁴, R.G. Gupta¹⁰⁴, S.P. Guzman⁴⁶, L. Gyulai¹⁴⁷, M.K. Habib¹¹⁰, C. Hadjidakis⁸⁰, G. Halimoglu⁷⁰, H. Hamagaki⁸⁵, G. Hamar¹⁴⁷, M. Hamid⁷, R. Hannigan¹²¹, M.R. Haque^{144,89}, A. Harlanderova¹¹⁰, J.W. Harris¹⁴⁸, A. Harton¹⁰, J.A. Hasenbichler³⁵, H. Hassan⁹⁹, D. Hatzifotiadou⁵⁵, P. Hauer⁴⁴, L.B. Havener¹⁴⁸, S. Hayashi¹³⁵, S.T. Heckel¹⁰⁸, E. Hellbär¹¹⁰, H. Helstrup³⁷, T. Herman³⁸, E.G. Hernandez⁴⁶, G. Herrera Corral⁹, F. Herrmann¹⁴⁶, K.F. Hetland³⁷, H. Hillemanns³⁵, C. Hills¹³⁰, B. Hippolyte¹³⁹, B. Hofman⁶⁴, B. Hohlweger⁹³, J. Honeremann¹⁴⁶, G.H. Hong¹⁴⁹, D. Horak³⁸, S. Hornung¹¹⁰, A. Horzyk², R. Hosokawa¹⁵, Y. Hou⁷, P. Hristov³⁵, C. Hughes¹³³, P. Huhn⁷⁰, T.J. Humanic¹⁰⁰, H. Hushnud¹¹², L.A. Husova¹⁴⁶, A. Hutson¹²⁷, D. Hutter⁴⁰, J.P. Iddon^{35,130}, R. Ilkaev¹¹¹, H. Ilyas¹⁴, M. Inaba¹³⁶,

G.M. Innocenti³⁵, M. Ippolitov⁹¹, A. Isakov^{38,98}, M.S. Islam¹¹², M. Ivanov¹¹⁰, V. Ivanov¹⁰¹, V. Izucheev⁹⁴, M. Jablonski², B. Jacak⁸², N. Jacazio³⁵, P.M. Jacobs⁸², S. Jadlovská¹¹⁹, J. Jadlovsky¹¹⁹, S. Jaelani⁶⁴, C. Jahnke^{124,123}, M.J. Jakubowska¹⁴⁴, A. Jalotra¹⁰⁴, M.A. Janik¹⁴⁴, T. Janson⁷⁶, M. Jercic¹⁰², O. Jevons¹¹³, A.A.P. Jimenez⁷¹, F. Jonas^{99,146}, P.G. Jones¹¹³, J.M. Jowett^{35,110}, J. Jung⁷⁰, M. Jung⁷⁰, A. Junique³⁵, A. Jusko¹¹³, J. Kaewjai¹¹⁸, P. Kalinak⁶⁶, A. Kalweit³⁵, V. Kaplin⁹⁶, S. Kar⁷, A. Karasu Uysal⁷⁹, D. Karatovic¹⁰², O. Karavichev⁶⁵, T. Karavicheva⁶⁵, P. Karczmarczyk¹⁴⁴, E. Karpechev⁶⁵, A. Kazantsev⁹¹, U. Kebschull⁷⁶, R. Keidel⁴⁸, D.L.D. Keijdener⁶⁴, M. Keil³⁵, B. Ketzer⁴⁴, Z. Khabanova⁹³, A.M. Khan⁷, S. Khan¹⁶, A. Khanzadeev¹⁰¹, Y. Kharlov⁹⁴, A. Khatun¹⁶, A. Khuntia¹²⁰, B. Kileng³⁷, B. Kim^{17,63}, C. Kim¹⁷, D.J. Kim¹²⁸, E.J. Kim⁷⁵, J. Kim¹⁴⁹, J.S. Kim⁴², J. Kim¹⁰⁷, J. Kim¹⁴⁹, J. Kim⁷⁵, M. Kim¹⁰⁷, S. Kim¹⁸, T. Kim¹⁴⁹, S. Kirsch⁷⁰, I. Kisel⁴⁰, S. Kiselev⁹⁵, A. Kisiel¹⁴⁴, J.P. Kitowski², J.L. Klay⁶, J. Klein³⁵, S. Klein⁸², C. Klein-Bösing¹⁴⁶, M. Kleiner⁷⁰, T. Klemenz¹⁰⁸, A. Kluge³⁵, A.G. Knospe¹²⁷, C. Kobdaj¹¹⁸, M.K. Köhler¹⁰⁷, T. Kollegger¹¹⁰, A. Kondratyev⁷⁷, N. Kondratyeva⁹⁶, E. Kondratyuk⁹⁴, J. König⁷⁰, S.A. Königstorfer¹⁰⁸, P.J. Konopka^{35,2}, G. Kornakov¹⁴⁴, S.D. Koryciak², L. Koska¹¹⁹, A. Kotliarov⁹⁸, O. Kovalenko⁸⁸, V. Kovalenko¹¹⁵, M. Kowalski¹²⁰, I. Králik⁶⁶, A. Kravčáková³⁹, L. Kreis¹¹⁰, M. Krivda^{113,66}, F. Krizek⁹⁸, K. Krizkova Gajdosova³⁸, M. Kroesen¹⁰⁷, M. Krüger⁷⁰, E. Kryshen¹⁰¹, M. Krzewicki⁴⁰, V. Kučera³⁵, C. Kuhn¹³⁹, P.G. Kuijer⁹³, T. Kumaoka¹³⁶, D. Kumar¹⁴³, L. Kumar¹⁰³, N. Kumar¹⁰³, S. Kundu^{35,89}, P. Kurashvili⁸⁸, A. Kurepin⁶⁵, A.B. Kurepin⁶⁵, A. Kuryakin¹¹¹, S. Kuschpil⁹⁸, J. Kvapil¹¹³, M.J. Kweon⁶³, J.Y. Kwon⁶³, Y. Kwon¹⁴⁹, S.L. La Pointe⁴⁰, P. La Rocca²⁷, Y.S. Lai⁸², A. Lakrathok¹¹⁸, M. Lamanna³⁵, R. Langoy¹³², K. Lapidus³⁵, P. Larionov^{35,53}, E. Laudi³⁵, L. Lautner^{35,108}, R. Lavicka³⁸, T. Lazareva¹¹⁵, R. Lea^{142,24,59}, J. Lehrbach⁴⁰, R.C. Lemmon⁹⁷, I. León Monzón¹²², E.D. Lesser¹⁹, M. Lettrich^{35,108}, P. Lévai¹⁴⁷, X. Li¹¹, X.L. Li⁷, J. Lien¹³², R. Lietava¹¹³, B. Lim¹⁷, S.H. Lim¹⁷, V. Lindenstruth⁴⁰, A. Lindner⁴⁹, C. Lippmann¹¹⁰, A. Liu¹⁹, D.H. Liu⁷, J. Liu¹³⁰, I.M. Lofnes²¹, V. Loginov⁹⁶, C. Loizides⁹⁹, P. Loncar³⁶, J.A. Lopez¹⁰⁷, X. Lopez¹³⁷, E. López Torres⁸, J.R. Luhder¹⁴⁶, M. Lunardon²⁸, G. Luparello⁶², Y.G. Ma⁴¹, A. Maevskaya⁶⁵, M. Mager³⁵, T. Mahmoud⁴⁴, A. Maire¹³⁹, M. Malaev¹⁰¹, N.M. Malik¹⁰⁴, Q.W. Malik²⁰, L. Malinina^{IV,77}, D. Mal'Kevich⁹⁵, N. Mallick⁵¹, P. Malzacher¹¹⁰, G. Mandaglio^{33,57}, V. Manko⁹¹, F. Manso¹³⁷, V. Manzari⁵⁴, Y. Mao⁷, J. Mares⁶⁸, G.V. Margagliotti²⁴, A. Margotti⁵⁵, A. Marín¹¹⁰, C. Markert¹²¹, M. Marquard⁷⁰, N.A. Martin¹⁰⁷, P. Martinengo³⁵, J.L. Martinez¹²⁷, M.I. Martínez⁴⁶, G. Martínez García¹¹⁷, S. Masciocchi¹¹⁰, M. Masera²⁵, A. Masoni⁵⁶, L. Massacrier⁸⁰, A. Mastroserio^{141,54}, A.M. Mathis¹⁰⁸, O. Matonoha⁸³, P.F.T. Matuoka¹²³, A. Matyja¹²⁰, C. Mayer¹²⁰, A.L. Mazuecos³⁵, F. Mazzaschi²⁵, M. Mazzilli³⁵, M.A. Mazzoni^{I,60}, J.E. Mdhului¹³⁴, A.F. Mechler⁷⁰, F. Meddi²², Y. Melikyan⁶⁵, A. Menchaca-Rocha⁷³, E. Meninno^{116,30}, A.S. Menon¹²⁷, M. Meres¹³, S. Mhlanga^{126,74}, Y. Miake¹³⁶, L. Micheletti^{61,25}, L.C. Migliorin¹³⁸, D.L. Mihaylov¹⁰⁸, K. Mikhaylov^{77,95}, A.N. Mishra¹⁴⁷, D. Miśkowiec¹¹⁰, A. Modak⁴, A.P. Mohanty⁶⁴, B. Mohanty⁸⁹, M. Mohisin Khan^{V,16}, M.A. Molander⁴⁵, Z. Moravcova⁹², C. Mordasini¹⁰⁸, D.A. Moreira De Godoy¹⁴⁶, L.A.P. Moreno⁴⁶, I. Morozov⁶⁵, A. Morsch³⁵, T. Mrnjavac³⁵, V. Muccifora⁵³, E. Mudnic³⁶, D. Mühlheim¹⁴⁶, S. Muhuri¹⁴³, J.D. Mulligan⁸², A. Mulliri²³, M.G. Munhoz¹²³, R.H. Munzer⁷⁰, H. Murakami¹³⁵, S. Murray¹²⁶, L. Musa³⁵, J. Musinsky⁶⁶, J.W. Myrcha¹⁴⁴, B. Naik^{134,50}, R. Nair⁸⁸, B.K. Nandi⁵⁰, R. Nania⁵⁵, E. Nappi⁵⁴, M.U. Naru¹⁴, A.F. Nassirpour⁸³, A. Nath¹⁰⁷, C. Nattrass¹³³, A. Neagu²⁰, L. Nellen⁷¹, S.V. Nesbo³⁷, G. Neskovic⁴⁰, D. Nesterov¹¹⁵, B.S. Nielsen⁹², S. Nikolaev⁹¹, S. Nikulin⁹¹, V. Nikulin¹⁰¹, F. Noferini⁵⁵, S. Noh¹², P. Nomokonov⁷⁷, J. Norman¹³⁰, N. Novitzky¹³⁶, P. Nowakowski¹⁴⁴, A. Nyman⁹¹, J. Nystrand²¹, M. Ogino⁸⁵, A. Ohlson⁸³, V.A. Okorokov⁹⁶, J. Olińczak¹⁴⁴, A.C. Oliveira Da Silva¹³³, M.H. Oliver¹⁴⁸, A. Onnerstad¹²⁸, C. Oppedisano⁶¹, A. Ortiz Velasquez⁷¹, T. Osako⁴⁷, A. Oskarsson⁸³, J. Otwinowski¹²⁰, M. Oya⁴⁷, K. Oyama⁸⁵, Y. Pachmayer¹⁰⁷, S. Padhan⁵⁰, D. Pagano^{142,59}, G. Paić⁷¹, A. Palasciano⁵⁴, J. Pan¹⁴⁵, S. Panebianco¹⁴⁰, P. Pareek¹⁴³, J. Park⁶³, J.E. Parkkila¹²⁸, S.P. Pathak¹²⁷, R.N. Patra^{104,35}, B. Paul²³, H. Pei⁷, T. Peitzmann⁶⁴, X. Peng⁷, L.G. Pereira⁷², H. Pereira Da Costa¹⁴⁰, D. Peresunko⁹¹, G.M. Perez⁸, S. Perrin¹⁴⁰, Y. Pestov⁵, V. Petráček³⁸, M. Petrovici⁴⁹, R.P. Pezzi^{117,72}, S. Piano⁶², M. Pikna¹³, P. Pillot¹¹⁷, O. Pinazza^{55,35}, L. Pinsky¹²⁷, C. Pinto²⁷, S. Pisano⁵³, M. Płoskoń⁸², M. Planinic¹⁰², F. Pliquett⁷⁰, M.G. Poghosyan⁹⁹, B. Polichtchouk⁹⁴, S. Politano³¹, N. Poljak¹⁰², A. Pop⁴⁹, S. Porteboeuf-Houssais¹³⁷, J. Porter⁸², V. Pozdniakov⁷⁷, S.K. Prasad⁴, R. Preghenella⁵⁵, F. Prino⁶¹, C.A. Pruneau¹⁴⁵, I. Pshenichnov⁶⁵, M. Puccio³⁵, S. Qiu⁹³, L. Quaglia²⁵, R.E. Quishpe¹²⁷, S. Ragoni¹¹³, A. Rakotozafindrabe¹⁴⁰, L. Ramello³², F. Rami¹³⁹, S.A.R. Ramirez⁴⁶, A.G.T. Ramos³⁴, T.A. Rancien⁸¹, R. Raniwala¹⁰⁵, S. Raniwala¹⁰⁵, S.S. Räsänen⁴⁵, R. Rath⁵¹, I. Ravasenga⁹³, K.F. Read^{99,133}, A.R. Redelbach⁴⁰, K. Redlich^{VI,88}, A. Rehman²¹, P. Reichelt⁷⁰, F. Reidt³⁵, H.A. Reme-ness³⁷, R. Renfordt⁷⁰, Z. Rescakova³⁹, K. Reygers¹⁰⁷, A. Riabov¹⁰¹, V. Riabov¹⁰¹, T. Richert⁸³, M. Richter²⁰, W. Riegler³⁵, F. Riggi²⁷, C. Ristea⁶⁹, M. Rodríguez Cahuantzi⁴⁶, K. Røed²⁰, R. Rogalev⁹⁴, E. Rogochaya⁷⁷, T.S. Rogoschinski⁷⁰, D. Rohr³⁵, D. Röhrich²¹, P.F. Rojas⁴⁶, P.S. Rokita¹⁴⁴, F. Ronchetti⁵³, A. Rosano^{33,57}, E.D. Rosas⁷¹, A. Rossi⁵⁸, A. Rotondi^{29,59}, A. Roy⁵¹, P. Roy¹¹², S. Roy⁵⁰, N. Rubini²⁶, O.V. Rueda⁸³, R. Rui²⁴, B. Ruyantsev⁷⁷, P.G. Russek², A. Rustamov⁹⁰, E. Ryabinkin⁹¹, Y. Ryabov¹⁰¹, A. Rybicki¹²⁰, H. Rytönen¹²⁸, W. Rzesza¹⁴⁴,

O.A.M. Saarimaki⁴⁵, R. Sadek¹¹⁷, S. Sadovsky⁹⁴, J. Saetre²¹, K. Šafařík³⁸, S.K. Saha¹⁴³, S. Saha⁸⁹, B. Sahoo⁵⁰, P. Sahoo⁵⁰, R. Sahoo⁵¹, S. Sahoo⁶⁷, D. Sahu⁵¹, P.K. Sahu⁶⁷, J. Saini¹⁴³, S. Sakai¹³⁶, S. Sambyal¹⁰⁴, V. Samsonov^{1,101,96}, D. Sarkar¹⁴⁵, N. Sarkar¹⁴³, P. Sarma⁴³, V.M. Sarti¹⁰⁸, M.H.P. Sas¹⁴⁸, J. Schambach^{99,121}, H.S. Scheid⁷⁰, C. Schiaua⁴⁹, R. Schicker¹⁰⁷, A. Schmah¹⁰⁷, C. Schmidt¹¹⁰, H.R. Schmidt¹⁰⁶, M.O. Schmidt³⁵, M. Schmidt¹⁰⁶, N.V. Schmidt^{99,70}, A.R. Schmier¹³³, R. Schotter¹³⁹, J. Schukraft³⁵, Y. Schutz¹³⁹, K. Schwarz¹¹⁰, K. Schweda¹¹⁰, G. Scioli²⁶, E. Scomparin⁶¹, J.E. Seger¹⁵, Y. Sekiguchi¹³⁵, D. Sekihata¹³⁵, I. Selyuzhenkov^{110,96}, S. Senyukov¹³⁹, J.J. Seo⁶³, D. Serebryakov⁶⁵, L. Šerkšnyte¹⁰⁸, A. Sevcenco⁶⁹, T.J. Shaba⁷⁴, A. Shabanov⁶⁵, A. Shabetai¹¹⁷, R. Shahoyan³⁵, W. Shaikh¹¹², A. Shangaraev⁹⁴, A. Sharma¹⁰³, H. Sharma¹²⁰, M. Sharma¹⁰⁴, N. Sharma¹⁰³, S. Sharma¹⁰⁴, U. Sharma¹⁰⁴, O. Sheibani¹²⁷, K. Shigaki⁴⁷, M. Shimomura⁸⁶, S. Shirinkin⁹⁵, Q. Shou⁴¹, Y. Sibiriak⁹¹, S. Siddhanta⁵⁶, T. Siemiarczuk⁸⁸, T.F. Silva¹²³, D. Silvermyr⁸³, G. Simonetti³⁵, B. Singh¹⁰⁸, R. Singh⁸⁹, R. Singh¹⁰⁴, R. Singh⁵¹, V.K. Singh¹⁴³, V. Singhal¹⁴³, T. Sinha¹¹², B. Sitar¹³, M. Sitta³², T.B. Skaali²⁰, G. Skorodumovs¹⁰⁷, M. Slupecki⁴⁵, N. Smirnov¹⁴⁸, R.J.M. Snellings⁶⁴, C. Soncco¹¹⁴, J. Song¹²⁷, A. Songmoolnak¹¹⁸, F. Soramel²⁸, S. Sorensen¹³³, I. Sputowska¹²⁰, J. Stachel¹⁰⁷, I. Stan⁶⁹, P.J. Steffanic¹³³, S.F. Stiefelmaier¹⁰⁷, D. Stocco¹¹⁷, I. Storehaug²⁰, M.M. Storetvedt³⁷, C.P. Stylianidis⁹³, A.A.P. Suaide¹²³, T. Sugitate⁴⁷, C. Suire⁸⁰, M. Sukhanov⁶⁵, M. Suljic³⁵, R. Sultanov⁹⁵, M. Šumbera⁹⁸, V. Sumberia¹⁰⁴, S. Sumowidagdo⁵², S. Swain⁶⁷, A. Szabo¹³, I. Szarka¹³, U. Tabassam¹⁴, S.F. Taghavi¹⁰⁸, G. Taillepiet¹³⁷, J. Takahashi¹²⁴, G.J. Tambave²¹, S. Tang^{137,7}, Z. Tang¹³¹, M. Tarhini¹¹⁷, M.G. Tarzila⁴⁹, A. Tauro³⁵, G. Tejada Muñoz⁴⁶, A. Telesca³⁵, L. Terlizzi²⁵, C. Terrevoli¹²⁷, G. Tersimonov³, S. Thakur¹⁴³, D. Thomas¹²¹, R. Tieulent¹³⁸, A. Tikhonov⁶⁵, A.R. Timmins¹²⁷, M. Tkacik¹¹⁹, A. Toia⁷⁰, N. Topilskaya⁶⁵, M. Toppi⁵³, F. Torres-Acosta¹⁹, T. Tork⁸⁰, S.R. Torres³⁸, A. Trifiró^{33,57}, S. Tripathy^{55,71}, T. Tripathy⁵⁰, S. Trogolo^{35,28}, G. Trombetta³⁴, V. Trubnikov³, W.H. Trzaska¹²⁸, T.P. Trzcinski¹⁴⁴, B.A. Trzeciak³⁸, A. Tumkin¹¹¹, R. Turrisi⁵⁸, T.S. Tveter²⁰, K. Ullaland²¹, A. Uras¹³⁸, M. Urioni^{59,142}, G.L. Usai²³, M. Vala³⁹, N. Valle^{59,29}, S. Vallero⁶¹, N. van der Kolk⁶⁴, L.V.R. van Doremalen⁶⁴, M. van Leeuwen⁹³, P. Vande Vyvre³⁵, D. Varga¹⁴⁷, Z. Varga¹⁴⁷, M. Varga-Kofarago¹⁴⁷, A. Vargas⁴⁶, M. Vasileiou⁸⁷, A. Vasiliev⁹¹, O. Vázquez Doce^{53,108}, V. Vechernin¹¹⁵, E. Vercellin²⁵, S. Vergara Limón⁴⁶, L. Vermunt⁶⁴, R. Vértesi¹⁴⁷, M. Verweij⁶⁴, L. Vickovic³⁶, Z. Vilakazi¹³⁴, O. Villalobos Baillie¹¹³, G. Vino⁵⁴, A. Vinogradov⁹¹, T. Virgili³⁰, V. Vislavicius⁹², A. Vodopyanov⁷⁷, B. Volkel³⁵, M.A. Völkl¹⁰⁷, K. Voloshin⁹⁵, S.A. Voloshin¹⁴⁵, G. Volpe³⁴, B. von Haller³⁵, I. Vorobyev¹⁰⁸, D. Voscek¹¹⁹, N. Vozniuk⁶⁵, J. Vrláková³⁹, B. Wagner²¹, C. Wang⁴¹, D. Wang⁴¹, M. Weber¹¹⁶, R.J.G.V. Weelden⁹³, A. Wegrzynek³⁵, S.C. Wenzel³⁵, J.P. Wessels¹⁴⁶, J. Wiechula⁷⁰, J. Wikne²⁰, G. Wilk⁸⁸, J. Wilkinson¹¹⁰, G.A. Willems¹⁴⁶, B. Windelband¹⁰⁷, M. Winn¹⁴⁰, W.E. Witt¹³³, J.R. Wright¹²¹, W. Wu⁴¹, Y. Wu¹³¹, R. Xu⁷, A.K. Yadav¹⁴³, S. Yalcin⁷⁹, Y. Yamaguchi⁴⁷, K. Yamakawa⁴⁷, S. Yang²¹, S. Yano⁴⁷, Z. Yin⁷, H. Yokoyama⁶⁴, I.-K. Yoo¹⁷, J.H. Yoon⁶³, S. Yuan²¹, A. Yuncu¹⁰⁷, V. Zaccolo²⁴, A. Zaman¹⁴, C. Zampolli³⁵, H.J.C. Zanolli⁶⁴, N. Zardoshti³⁵, A. Zarochentsev¹¹⁵, P. Závada⁶⁸, N. Zaviyalov¹¹¹, M. Zhalov¹⁰¹, B. Zhang⁷, S. Zhang⁴¹, X. Zhang⁷, Y. Zhang¹³¹, V. Zhrebchevskii¹¹⁵, Y. Zhi¹¹, N. Zhigareva⁹⁵, D. Zhou⁷, Y. Zhou⁹², J. Zhu^{7,110}, Y. Zhu⁷, A. Zichichi²⁶, G. Zinovjev³, N. Zurlo^{142,59}

Affiliation notes

^I Deceased

^{II} Also at: Italian National Agency for New Technologies, Energy and Sustainable Economic Development (ENEA), Bologna, Italy

^{III} Also at: Dipartimento DET del Politecnico di Torino, Turin, Italy

^{IV} Also at: M.V. Lomonosov Moscow State University, D.V. Skobeltsyn Institute of Nuclear, Physics, Moscow, Russia

^V Also at: Department of Applied Physics, Aligarh Muslim University, Aligarh, India

^{VI} Also at: Institute of Theoretical Physics, University of Wrocław, Poland

Collaboration Institutes

¹ A.I. Alikhanyan National Science Laboratory (Yerevan Physics Institute) Foundation, Yerevan, Armenia

² AGH University of Science and Technology, Cracow, Poland

³ Bogolyubov Institute for Theoretical Physics, National Academy of Sciences of Ukraine, Kiev, Ukraine

⁴ Bose Institute, Department of Physics and Centre for Astroparticle Physics and Space Science (CAPSS), Kolkata, India

⁵ Budker Institute for Nuclear Physics, Novosibirsk, Russia

⁶ California Polytechnic State University, San Luis Obispo, California, United States

- ⁷ Central China Normal University, Wuhan, China
- ⁸ Centro de Aplicaciones Tecnológicas y Desarrollo Nuclear (CEADEN), Havana, Cuba
- ⁹ Centro de Investigación y de Estudios Avanzados (CINVESTAV), Mexico City and Mérida, Mexico
- ¹⁰ Chicago State University, Chicago, Illinois, United States
- ¹¹ China Institute of Atomic Energy, Beijing, China
- ¹² Chungbuk National University, Cheongju, Republic of Korea
- ¹³ Comenius University Bratislava, Faculty of Mathematics, Physics and Informatics, Bratislava, Slovakia
- ¹⁴ COMSATS University Islamabad, Islamabad, Pakistan
- ¹⁵ Creighton University, Omaha, Nebraska, United States
- ¹⁶ Department of Physics, Aligarh Muslim University, Aligarh, India
- ¹⁷ Department of Physics, Pusan National University, Pusan, Republic of Korea
- ¹⁸ Department of Physics, Sejong University, Seoul, Republic of Korea
- ¹⁹ Department of Physics, University of California, Berkeley, California, United States
- ²⁰ Department of Physics, University of Oslo, Oslo, Norway
- ²¹ Department of Physics and Technology, University of Bergen, Bergen, Norway
- ²² Dipartimento di Fisica dell'Università 'La Sapienza' and Sezione INFN, Rome, Italy
- ²³ Dipartimento di Fisica dell'Università and Sezione INFN, Cagliari, Italy
- ²⁴ Dipartimento di Fisica dell'Università and Sezione INFN, Trieste, Italy
- ²⁵ Dipartimento di Fisica dell'Università and Sezione INFN, Turin, Italy
- ²⁶ Dipartimento di Fisica e Astronomia dell'Università and Sezione INFN, Bologna, Italy
- ²⁷ Dipartimento di Fisica e Astronomia dell'Università and Sezione INFN, Catania, Italy
- ²⁸ Dipartimento di Fisica e Astronomia dell'Università and Sezione INFN, Padova, Italy
- ²⁹ Dipartimento di Fisica e Nucleare e Teorica, Università di Pavia, Pavia, Italy
- ³⁰ Dipartimento di Fisica 'E.R. Caianiello' dell'Università and Gruppo Collegato INFN, Salerno, Italy
- ³¹ Dipartimento DISAT del Politecnico and Sezione INFN, Turin, Italy
- ³² Dipartimento di Scienze e Innovazione Tecnologica dell'Università del Piemonte Orientale and INFN Sezione di Torino, Alessandria, Italy
- ³³ Dipartimento di Scienze MIFT, Università di Messina, Messina, Italy
- ³⁴ Dipartimento Interateneo di Fisica 'M. Merlin' and Sezione INFN, Bari, Italy
- ³⁵ European Organization for Nuclear Research (CERN), Geneva, Switzerland
- ³⁶ Faculty of Electrical Engineering, Mechanical Engineering and Naval Architecture, University of Split, Split, Croatia
- ³⁷ Faculty of Engineering and Science, Western Norway University of Applied Sciences, Bergen, Norway
- ³⁸ Faculty of Nuclear Sciences and Physical Engineering, Czech Technical University in Prague, Prague, Czech Republic
- ³⁹ Faculty of Science, P.J. Šafárik University, Košice, Slovakia
- ⁴⁰ Frankfurt Institute for Advanced Studies, Johann Wolfgang Goethe-Universität Frankfurt, Frankfurt, Germany
- ⁴¹ Fudan University, Shanghai, China
- ⁴² Gangneung-Wonju National University, Gangneung, Republic of Korea
- ⁴³ Gauhati University, Department of Physics, Guwahati, India
- ⁴⁴ Helmholtz-Institut für Strahlen- und Kernphysik, Rheinische Friedrich-Wilhelms-Universität Bonn, Bonn, Germany
- ⁴⁵ Helsinki Institute of Physics (HIP), Helsinki, Finland
- ⁴⁶ High Energy Physics Group, Universidad Autónoma de Puebla, Puebla, Mexico
- ⁴⁷ Hiroshima University, Hiroshima, Japan
- ⁴⁸ Hochschule Worms, Zentrum für Technologietransfer und Telekommunikation (ZTT), Worms, Germany
- ⁴⁹ Horia Hulubei National Institute of Physics and Nuclear Engineering, Bucharest, Romania
- ⁵⁰ Indian Institute of Technology Bombay (IIT), Mumbai, India
- ⁵¹ Indian Institute of Technology Indore, Indore, India
- ⁵² Indonesian Institute of Sciences, Jakarta, Indonesia
- ⁵³ INFN, Laboratori Nazionali di Frascati, Frascati, Italy
- ⁵⁴ INFN, Sezione di Bari, Bari, Italy
- ⁵⁵ INFN, Sezione di Bologna, Bologna, Italy
- ⁵⁶ INFN, Sezione di Cagliari, Cagliari, Italy
- ⁵⁷ INFN, Sezione di Catania, Catania, Italy
- ⁵⁸ INFN, Sezione di Padova, Padova, Italy

- 59 INFN, Sezione di Pavia, Pavia, Italy
- 60 INFN, Sezione di Roma, Rome, Italy
- 61 INFN, Sezione di Torino, Turin, Italy
- 62 INFN, Sezione di Trieste, Trieste, Italy
- 63 Inha University, Incheon, Republic of Korea
- 64 Institute for Gravitational and Subatomic Physics (GRASP), Utrecht University/Nikhef, Utrecht, Netherlands
- 65 Institute for Nuclear Research, Academy of Sciences, Moscow, Russia
- 66 Institute of Experimental Physics, Slovak Academy of Sciences, Košice, Slovakia
- 67 Institute of Physics, Homi Bhabha National Institute, Bhubaneswar, India
- 68 Institute of Physics of the Czech Academy of Sciences, Prague, Czech Republic
- 69 Institute of Space Science (ISS), Bucharest, Romania
- 70 Institut für Kernphysik, Johann Wolfgang Goethe-Universität Frankfurt, Frankfurt, Germany
- 71 Instituto de Ciencias Nucleares, Universidad Nacional Autónoma de México, Mexico City, Mexico
- 72 Instituto de Física, Universidade Federal do Rio Grande do Sul (UFRGS), Porto Alegre, Brazil
- 73 Instituto de Física, Universidad Nacional Autónoma de México, Mexico City, Mexico
- 74 iThemba LABS, National Research Foundation, Somerset West, South Africa
- 75 Jeonbuk National University, Jeonju, Republic of Korea
- 76 Johann-Wolfgang-Goethe Universität Frankfurt Institut für Informatik, Fachbereich Informatik und Mathematik, Frankfurt, Germany
- 77 Joint Institute for Nuclear Research (JINR), Dubna, Russia
- 78 Korea Institute of Science and Technology Information, Daejeon, Republic of Korea
- 79 KTO Karatay University, Konya, Turkey
- 80 Laboratoire de Physique des 2 Infinis, Irène Joliot-Curie, Orsay, France
- 81 Laboratoire de Physique Subatomique et de Cosmologie, Université Grenoble-Alpes, CNRS-IN2P3, Grenoble, France
- 82 Lawrence Berkeley National Laboratory, Berkeley, California, United States
- 83 Lund University Department of Physics, Division of Particle Physics, Lund, Sweden
- 84 Moscow Institute for Physics and Technology, Moscow, Russia
- 85 Nagasaki Institute of Applied Science, Nagasaki, Japan
- 86 Nara Women's University (NWU), Nara, Japan
- 87 National and Kapodistrian University of Athens, School of Science, Department of Physics, Athens, Greece
- 88 National Centre for Nuclear Research, Warsaw, Poland
- 89 National Institute of Science Education and Research, Homi Bhabha National Institute, Jatni, India
- 90 National Nuclear Research Center, Baku, Azerbaijan
- 91 National Research Centre Kurchatov Institute, Moscow, Russia
- 92 Niels Bohr Institute, University of Copenhagen, Copenhagen, Denmark
- 93 Nikhef, National institute for subatomic physics, Amsterdam, Netherlands
- 94 NRC Kurchatov Institute IHEP, Protvino, Russia
- 95 NRC «Kurchatov» Institute - ITEP, Moscow, Russia
- 96 NRNU Moscow Engineering Physics Institute, Moscow, Russia
- 97 Nuclear Physics Group, STFC Daresbury Laboratory, Daresbury, United Kingdom
- 98 Nuclear Physics Institute of the Czech Academy of Sciences, Řež u Prahy, Czech Republic
- 99 Oak Ridge National Laboratory, Oak Ridge, Tennessee, United States
- 100 Ohio State University, Columbus, Ohio, United States
- 101 Petersburg Nuclear Physics Institute, Gatchina, Russia
- 102 Physics department, Faculty of science, University of Zagreb, Zagreb, Croatia
- 103 Physics Department, Panjab University, Chandigarh, India
- 104 Physics Department, University of Jammu, Jammu, India
- 105 Physics Department, University of Rajasthan, Jaipur, India
- 106 Physikalisches Institut, Eberhard-Karls-Universität Tübingen, Tübingen, Germany
- 107 Physikalisches Institut, Ruprecht-Karls-Universität Heidelberg, Heidelberg, Germany
- 108 Physik Department, Technische Universität München, Munich, Germany
- 109 Politecnico di Bari and Sezione INFN, Bari, Italy
- 110 Research Division and ExtreMe Matter Institute EMMI, GSI Helmholtzzentrum für Schwerionenforschung GmbH, Darmstadt, Germany
- 111 Russian Federal Nuclear Center (VNIIEF), Sarov, Russia

- 112 Saha Institute of Nuclear Physics, Homi Bhabha National Institute, Kolkata, India
- 113 School of Physics and Astronomy, University of Birmingham, Birmingham, United Kingdom
- 114 Sección Física, Departamento de Ciencias, Pontificia Universidad Católica del Perú, Lima, Peru
- 115 St. Petersburg State University, St. Petersburg, Russia
- 116 Stefan Meyer Institut für Subatomare Physik (SMI), Vienna, Austria
- 117 SUBATECH, IMT Atlantique, Université de Nantes, CNRS-IN2P3, Nantes, France
- 118 Suranaree University of Technology, Nakhon Ratchasima, Thailand
- 119 Technical University of Košice, Košice, Slovakia
- 120 The Henryk Niewodniczanski Institute of Nuclear Physics, Polish Academy of Sciences, Cracow, Poland
- 121 The University of Texas at Austin, Austin, Texas, United States
- 122 Universidad Autónoma de Sinaloa, Culiacán, Mexico
- 123 Universidade de São Paulo (USP), São Paulo, Brazil
- 124 Universidade Estadual de Campinas (UNICAMP), Campinas, Brazil
- 125 Universidade Federal do ABC, Santo Andre, Brazil
- 126 University of Cape Town, Cape Town, South Africa
- 127 University of Houston, Houston, Texas, United States
- 128 University of Jyväskylä, Jyväskylä, Finland
- 129 University of Kansas, Lawrence, Kansas, United States
- 130 University of Liverpool, Liverpool, United Kingdom
- 131 University of Science and Technology of China, Hefei, China
- 132 University of South-Eastern Norway, Tonsberg, Norway
- 133 University of Tennessee, Knoxville, Tennessee, United States
- 134 University of the Witwatersrand, Johannesburg, South Africa
- 135 University of Tokyo, Tokyo, Japan
- 136 University of Tsukuba, Tsukuba, Japan
- 137 Université Clermont Auvergne, CNRS/IN2P3, LPC, Clermont-Ferrand, France
- 138 Université de Lyon, CNRS/IN2P3, Institut de Physique des 2 Infinis de Lyon, Lyon, France
- 139 Université de Strasbourg, CNRS, IPHC UMR 7178, F-67000 Strasbourg, France, Strasbourg, France
- 140 Université Paris-Saclay Centre d'Etudes de Saclay (CEA), IRFU, Département de Physique Nucléaire (DPhN), Saclay, France
- 141 Università degli Studi di Foggia, Foggia, Italy
- 142 Università di Brescia, Brescia, Italy
- 143 Variable Energy Cyclotron Centre, Homi Bhabha National Institute, Kolkata, India
- 144 Warsaw University of Technology, Warsaw, Poland
- 145 Wayne State University, Detroit, Michigan, United States
- 146 Westfälische Wilhelms-Universität Münster, Institut für Kernphysik, Münster, Germany
- 147 Wigner Research Centre for Physics, Budapest, Hungary
- 148 Yale University, New Haven, Connecticut, United States
- 149 Yonsei University, Seoul, Republic of Korea